Sensory neuron-derived TAFA4 promotes macrophage tissue repair functions

Guillaume Hoeffel, Guilhaume Debroas, Anais Roger, Rafaëlle Rossignol, Jordi Gouilly, Caroline Laprie, Lionel Chasson, Pierre Vincent Barbon, Anais Balsamo, Ana Reynders, et al.

Sensory neuron-derived TAFA4 promotes macrophage tissue repair functions

Guillaume Hoeffel[1*#], Guilhaume Debroas[1*], Anais Roger[1], Rafaelle Rossignol[1], Jordi Gouilly[1], Caroline Laprie[1], Lionel Chasson[1], Pierre Vincent Barbon[1], Anais Balsamo[1], Ana Reynders[2], Aziz Moqrich[2] and Sophie Ugolini[1#]

[1] Aix Marseille Univ, CNRS, INSERM, CIML, Centre d'Immunologie de Marseille-Luminy, Marseille, France

[2] Aix Marseille Univ, CNRS, IBDM, Institut de Biologie du Développement de Marseille, Marseille, France

[*]Equal contributions

[#]Corresponding authors: hoeffel@ciml.univ-mrs.fr; ugolini@ciml.univ-mrs.fr

Keywords: Monocytes, macrophages, sensory neurons, neuropeptides, tissue repair, skin fibrosis, TAFA4, GINIP

Running title: TAFA4 triggers IL-10 production by dermal macrophages and promotes skin repair

Summary

Inflammation is a defense response to tissue damage requiring tight regulation to prevent impaired healing. Tissue-resident macrophages play a key role in tissue repair[1] but the precise molecular mechanisms regulating the balance between inflammatory and pro-repair macrophage responses during healing remain poorly understood. We demonstrate here a major role of sensory neurons in promoting macrophage tissue repair functions. In a sunburn-like model of skin damage, the conditional ablation of sensory neurons expressing the Gαi-interacting protein (GINIP) resulted in defective tissue regeneration, and dermal fibrosis. Dissection of the underlying molecular mechanisms revealed a crucial role for the neuropeptide TAFA4, produced in the skin by C-low threshold mechanoreceptors (C-LTMR), a subset of GINIP$^+$ neurons. TAFA4 modulated the inflammatory profile of macrophages directly *in vitro*. *In vivo* analyses in *Tafa4*-deficient mice revealed that TAFA4 promoted IL-10 production by dermal macrophages after UV-induced skin damage. This TAFA4/IL-10 axis also ensured the survival and maintenance of IL-10$^+$Tim4$^+$ dermal macrophages, resolving skin inflammation and promoting tissue regeneration. These results reveal a new neuroimmune regulatory pathway driven by the neuropeptide TAFA4 that promotes macrophage anti-inflammatory functions and prevents fibrosis upon tissue damage, creating new therapeutic perspectives for inflammatory diseases.

Main text

Skin overexposure to ultraviolet (UV) light causes sunburn, characterized by epidermis destruction and inflammation of the underlying dermal papilla[2]. Such tissue damage induces a complex inflammatory response, requiring tight regulation to prevent persistent injury. Sunburn is also characterized by a transient phase of painful hypersensitivity, mediated by the activation of specialized skin-innervating sensory neurons[3,4]. Studies of other pathological cutaneous conditions have shown that the peripheral nervous system regulates cutaneous inflammatory processes[3,5-9]. Most studies have focused on the roles of TRPV1$^+$ peptidergic primary sensory neurons and the neuropeptide CGRP[3,5-7,9] (calcitonin gene-related peptide). However, the potential immunoregulatory role of non-peptidergic C-fibers expressing GINIP[10] remains unknown.

GINIP$^+$ neurons prevent UV-induced skin fibrosis

We analyzed the role of somatosensory neurons in tissue repair in mouse ears exposed to UV-C radiation, an experimental model of sunburn (**Fig. 1a**). We assessed the expression of genes associated with tissue inflammation and repair in skin from wild-type (WT) mice, following UV overexposure. Genes encoding inflammatory molecules, such as *Il-1β* and *Tnfα*, were upregulated until day 7 post-UV irradiation (pi), whereas pro-repair genes, such as *Col1a1* and *Retlna*, were upregulated from day 14 until day 35 pi, defining the resolution/repair phase of this model (**Extended data Fig. 1a**).

We analyzed the consequences for the somatosensory nervous system of skin overexposure to UV light. Most of the neurons responsible for detecting noxious stimuli and eliciting pain perception express the sodium channel Nav1.8[11-13], and have cell

bodies in the dorsal root ganglia (DRGs) or trigeminal ganglion. We monitored the expression of ATF3 (Activating Transcription Factor 3), a transcription factor used as a proxy for neuronal injury and activation[14], in DRGs after skin exposure to UV. *Atf3* expression significantly increased in C2/C3 DRGs, which specifically innervate ear skin (**Fig. 1b, Extended data Fig. 1b-d**).

We determined the phenotype of $ATF3^+$ DRG neurons, by immunofluorescence staining. Very few of these neurons co-expressed CGRP pi, whereas up to 50% co-expressed GINIP (**Fig. 1c, d, Extended data Figure 1e, f**), suggesting that UV-induced skin inflammation essentially affects $GINIP^+$ somatosensory neurons.

We therefore investigated the role of these $Nav1.8^+GINIP^+$ neurons ($GINIP^+$ neurons) in tissue repair, by conditional depletion in the GINIP-DTR model[10,15] (**Extended data Fig. 2a-c**). Between days 5 and 35 pi, ear skin was significantly thicker in GINIP-DTR mice than in control DTR ("control") littermates (**Fig. 1e**). Macroscopic analysis also revealed greater redness, tissue shrinkage and signs of necrosis leading to ear tissue loss in GINIP-DTR mice (**Fig. 1f)**. These skin lesions were not associated with an increase in scratching in GINIP-DTR mice (**Extended data Fig. 2d**). Histological analysis showed similar steady-state skin structures in GINIP-DTR and control littermates. By contrast, 35 days pi, GINIP-DTR mice displayed marked pinna thickening, with an increase in horizontally oriented collagen fiber deposition, persistent leukocytic infiltration and focal auricular cartilage obliteration, whereas control mice presented signs of skin healing (**Fig. 1g-j, Extended data Fig. 2e-j**). Thus, $GINIP^+$ neurons prevent skin over-inflammation and fibrosis after UV irradiation.

Impaired macrophage response in GINIP-DTR mice

We investigated whether the profound tissue repair defect of GINIP-DTR mice was linked to dysregulation of the cutaneous immune response. The absolute numbers of dendritic cells (DC), Langerhans cells (LC), mast cells, lymphoid cells and granulocytes were similar in GINIP-DTR and control mice, at steady state and 14 days pi, whereas GINIP-DTR mice had fewer monocytes/macrophages (Mo/Mϕ) than control mice pi (**Extended data Fig. 3a-d**). None of these immune cells expressed DTR in GINIP-DTR mice, and their numbers were unaffected by DT treatment in homeostatic conditions (**Extended data Fig. 3b-d, f)**.

Macrophages regulate all stages of tissue repair[1], and dysregulation of their homeostasis can lead to chronic inflammation, excessive collagen deposition and hypertrophic/fibrotic scars[1]. Dermal resident Mϕ expressing CD206 were observed near GINIP$^+$ nerve terminals, suggesting possible functional interaction (**Fig. 2a-b, Extended data Fig. 3g**). We analyzed the dermal Mo/Mϕ response upon UV overexposure. Tissue-resident Mϕ emerge either during embryonic development[16-18] or differentiate postnatally from circulating monocytes[18,19]. Upon inflammation, monocyte subsets[20], including "classical" Ly6C$^+$ monocytes (Mo), "patrolling" Ly6C^{lo} monocytes (PMo) and "intermediate" Ly6C$^+$MHC-II$^+$ monocytes (Int. Mo), can generate short-lived MHC-II$^+$ monocyte-derived DC (MoDC) and monocyte-derived CD64$^+$CD206$^-$ inflammatory macrophages (Inflam Mϕ). We identified eight Mo/Mϕ subsets based on differential expression of CCR2, CD64, Ly6C, MHC-II, CD206 and Tim4 (**Fig. 2c, Extended data Fig. 4a-c).** Their steady-state distributions were similar in the skin of GINIP-DTR and control mice (**Fig. 2e, f, Extended data Fig. 4d-h**). By contrast, absolute numbers of Tim4$^+$ dermal Mϕ were very low from days 3 to 14 pi in the skin of GINIP-DTR mice (**Fig. 2c-e**), whereas Ly6C$^+$Mo recruitment increased on day 3 pi (**Extended data Fig. 4d**). This influx of Ly6C$^+$Mo was associated with

increases in Inflam Mϕ numbers in GINIP-DTR mice from days 3 to 14 pi (**Fig. 2f),** consistent with the stronger skin inflammation observed in these mice (**Fig. 1e**). By contrast, the expansion of DN and MHC-II$^+$ dermal Mϕ subsets was little affected by the absence of GINIP$^+$ neurons (**Extended data Fig. 4e-h**). Thus, signals from GINIP$^+$ sensory neurons promote Tim4$^+$ dermal Mϕ maintenance and control Inflam Mϕ responses following UV-induced skin damage.

TAFA4 promotes skin repair upon UV exposure

We investigated the mechanisms underlying the immunomodulatory and pro-repair role of GINIP$^+$ neurons. GINIP is expressed by two somatosensory neuron subsets: GINIP$^+$/IB4$^+$ neurons, which also express MRGPRD and selectively innervate the epidermis, and GINIP$^+$/IB4$^-$ neurons, which express TAFA4, TH and VGLUT3, markers of the C-low-threshold mechanoreceptors (C-LTMRs) selectively innervating hair follicles[10,21] (**Extended data Fig. 5a-c**). Binding to isolectin-B4 (IB4) and TAFA4 can be used to distinguish between these subsets in DRGs[10,22,23]. We generated anti-TAFA4 monoclonal antibodies (**Extended data Fig. 5d, g**), for C-LTMR identification. As expected, TAFA4$^+$, TH$^+$ and IB4$^+$ neurons were ablated in GINIP-DTR mice, whereas CGRP$^+$ neurons were spared (**Extended data Fig. 2b**). DRG staining showed that 10-20% of ATF3$^+$ neurons were IB4$^+$ and 20-50% were TAFA4$^+$ (**Fig. 3a, b, Extended data Fig. 5e, f**), suggesting potential roles for these subsets of GINIP$^+$ neurons in regulating UV-induced skin inflammation.

C-LTMRs mediate two opposing aspects of touch sensation: pleasantness and injury-induced mechanical pain[10,22]. TAFA4 is a secreted protein[24] that can modulate injury-induced mechanical hypersensitivity and chemical pain in mice[22]. TAFA4 promotes

148 human macrophage chemotaxis *in vitro*[25], but its impact on myeloid cell responses *in*
149 *vivo* remains unknown.
150 We established an ELISA for TAFA4 detection in tissues. UV exposure induced
151 increases in TAFA4 levels in WT mouse DRGs and skin (**Fig. 3c, Extended data Fig.**
152 **5h**). We investigated the cellular source of TAFA4 in skin. Consistent with publicly
153 available database (http://www.immgen.org; http://biogps.org), *Tafa4* (*Fam19a4*)
154 transcription was observed in DRGs, but not in the blood, gut, lung or skin (**Extended**
155 **data Fig. 5i**). *Tafa4* transcription has been reported in human Mϕ following LPS
156 stimulation [25]. However, we detected no *Tafa4* transcripts in BM-derived macrophages
157 (BMDM) activated with LPS (+/-TAFA4) or in sorted $CD206^+$ dermal Mϕ on days 0
158 and 7 pi (**Extended data Fig. 5j**). *Tafa4* mRNA was undetectable in the skin, even after
159 UV exposure, but abundant in DRGs pi (**Extended data Fig.1a, 5k**). These data
160 strongly suggest that *Tafa4* is transcribed only in DRG neuron cell bodies, with protein
161 release into the skin via C-LTMR nerve endings.
162 We investigated the possible role of TAFA4 in regulating tissue regeneration pi, by
163 studying *Tafa4*-KO mice[22]. From days 14 to 35 pi, *Tafa-4*-KO mice had thicker ear skin
164 than control littermates, suggesting defective resolution of skin inflammation in the
165 absence of TAFA4 (**Extended data Fig. 6a)**. No histological change in the skin of
166 *Tafa4*-KO mice was observed in homeostatic conditions. By contrast, 35 days pi,
167 leukocyte infiltration score and epidermal thickness were higher in *Tafa4*-KO mice,
168 which displayed more extensive, persistent dermal fibrosis (**Extended data Fig. 6b, c**).
169 Picro Sirius Red staining revealed characteristic excessive type 1 collagen deposition
170 in unresolved fibrotic scars in the dermis of *Tafa4*-KO mice (**Fig. 3d, e**). Thus, like
171 GINIP-DTR mice, *Tafa4*-KO mice presented pathological fibrosis, suggesting a
172 requirement for the neuropeptide TAFA4, produced by C-LTMRs, for skin repair pi.

TAFA4 regulates dermal macrophage IL-10 production

We investigated the mechanisms by which TAFA4 regulates skin repair. We monitored inflammatory cytokine and chemokine concentrations in skin from *Tafa4*-KO mice and control littermates from days 0 to 35 pi. TNFα, IL-1β, IL-6, CCL2, CCL4 and CXCL1 (**Fig. 3f, Extended data Fig. 6d)** levels decreased between days 7 and 10 pi in control mice, but remained higher in *Tafa4*-KO mice**.** By contrast, expression levels of the anti-inflammatory cytokine IL-10 were lower in the skin of *Tafa4*-KO mice pi (**Fig. 3g, Extended data Fig. 6d**). Resolution of the inflammatory phase was therefore impaired in the absence of TAFA4.

IL-10 is a potent anti-inflammatory molecule. We hypothesized that impaired IL-10 production might underlie the observed dysregulation of skin repair in UV-exposed *Tafa4*-KO mice. Intracellular staining and analyses in IL-10-GFP reporter mice identified resident Mϕ and mast cells [26] as the main producers of IL-10, with regulatory T cells (Tregs) producing only small amounts (**Extended data Fig. 6e-i**). Mast cell numbers and IL-10 production decreased strongly on day 3 pi (**Extended data Fig. 6j-m**). TAFA4 deficiency was not associated with modulation of IL-10 production by Tregs and mast cells (**Extended data Fig. 6i-m**). By contrast, *Il10* levels in sorted $CD206^+$ dermal Mϕ were lower in *Tafa4*-KO mice than in controls on days 7 and 10 pi (**Fig. 3h**). Intracellular staining confirmed that TAFA4 was required for the upregulation of IL-10 production in all $CD206^+$ Mϕ subsets after UV overexposure, with $Tim4^+$ Mϕ producing more IL-10 than DN and $MHC\text{-}II^+$ Mϕ (**Extended data Fig. 7a-c**).

We investigated whether TAFA4 regulated Mϕ activation directly. BMDM or purified peritoneal Mϕ (ThioMϕ) were activated with LPS in the presence or absence of TAFA4.

198 *Tnfα, Il1β* and *Il6* transcripts were significantly downregulated, whereas *Il10*
199 transcripts were upregulated by TAFA4 (**Fig. 3i, Extended data Fig.7e**). Together,
200 these data suggest that the TAFA4-mediated regulation of IL-10 production in the skin
201 upon UV-exposure is mediated essentially through the regulation of dermal
202 Mϕ functions.
203 Formyl peptide receptor 1 (FPR1) has been described as a TAFA4 receptor inducing
204 the chemotaxis of human Mϕ and transfected cell lines *in vitro*[25]. We observed no
205 chemotactic effect of TAFA4 on mouse BMDM or isolated peritoneal Mϕ *in vitro*
206 (**Extended data Fig. 7d and data not shown).** Consistently *in vivo,* monocyte-derived
207 cell recruitment pi was not reduced in GINIP-DTR mice (**Extended data Figure 4d**).
208 Moreover, TAFA4 had a similar immunoregulatory effect on BMDM from FPR1-KO
209 and WT mice showing that at least one other unknown receptor drives the functional
210 effect of TAFA4 on Mϕ (**Extended data Fig. 7f).** Thus, TAFA4 can regulate the
211 inflammatory profile of Mϕ directly, in an FPR1-independent manner. It will be
212 important to determine whether macrophage regulation by TAFA4 differs between
213 mice and humans.
214
215 **A TAFA4-IL10-Tim4^{+} macrophage axis promotes tissue repair**
216 We then investigated whether TAFA4 affected the dynamics between dermal resident
217 Mϕ and newly recruited monocyte-derived cells during repair. We first performed a
218 lineage-tracing analysis, tracking the fate of CX3CR1^{+} embryonic Mϕ precursors using
219 the tamoxifen-dependent CX3CR1^{CreERT2}:R26-YFP mouse model[27]. YFP expression
220 was selectively induced in CX3CR1^{+} cells on day 16.5 of embryonic development. In
221 adult mice under homeostatic conditions, the MHC-II^{+} and DN dermal Mϕ subsets only
222 weakly expressed YFP (**Extended data Fig. 8a, b)**. By contrast, 20% of Tim4^{+} Mϕ

were YFP$^+$, like LCs [28], suggesting that Tim4$^+$ Mϕ are mostly *bona fide* embryo-derived cells.

We then assessed the contribution of monocytes to the various dermal Mo/Mϕ subsets, by generating shield-irradiated BM chimeras (**Extended data Fig. 8c).** As expected, two months after CD45.1 BM reconstitution in CD45.2 recipients, 90% of blood monocytes were CD45.1$^+$, whereas microglia were entirely of recipient (CD45.2$^+$) origin. Under homeostatic conditions, dermal Ly6C$^+$Mo, Int Mo, PMo, MoDC and Inflam Mϕ were mostly CD45.1$^+$, confirming their BM origin, whereas Tim4$^+$ Mϕ were CD45.2$^+$, demonstrating their self-maintenance over time independently of circulating monocytes (**Extended data Fig. 8d**). However, 120 days pi, the CD45.1 chimerism of DN and Tim4 Mϕ increased (**Extended data Fig. 8e**), showing that monocytes recruited pi acquired a resident-like Mϕ phenotype with self-renewing capacity.

We then generated shield-irradiated BM chimeras, using WT or *Tafa4*-KO (both CD45.2) recipient mice (**Fig. 4a-f, Extended data Fig. 8f-h).** Intracellular staining on day 7 pi revealed that IL-1β expression was mostly associated with monocyte-derived cells, whereas TNFα expression was restricted essentially to Inflam Mϕ (**Fig. 4c**). The number of Inflam Mϕ cells in *Tafa4*-KO chimeric mice was higher than that in control chimeras, suggesting that TAFA4 reduces the number of newly derived Inflam Mϕ (**Fig. 4d**). Tim4$^+$ Mϕ were the predominant CD45.2$^+$ population in both chimeras (**Fig. 4b, c**), consistent with our previous analysis. Tim4$^+$ Mϕ produced large amounts of IL-10, but no IL-1β or TNFα (**Fig. 4c**), highlighting their anti-inflammatory function. TAFA4 deficiency had little effect on DN and MHC-II$^+$ Mϕ homeostasis pi (**Extended data Fig. 8h**). By contrast, the absolute number of CD45.2$^+$ Tim4$^+$ Mϕ, which was

similar in both chimeras under homeostatic conditions, strongly decreased in *Tafa4*-KO recipient mice pi (**Fig. 4e left).** Overall CD45.1 chimerism levels in Tim4$^+$ Mϕ revealed that CD45.2$^+$ Tim4$^+$ Mϕ were replaced by CD45.1$^+$ monocyte differentiation to a greater extent in *Tafa4*-KO than in WT recipients (**Fig. 4e right**). However, the overall Tim4$^+$ Mϕ pool expanded to a lesser extent in the absence of TAFA4 (**Fig. 4f**), suggesting that both embryo-derived, and monocyte-derived Tim4$^+$ Mϕ require TAFA4 for survival pi. Consistently, the frequency of apoptotic Annexin$^+$Tim4$^+$ cells in UV-exposed skin was higher for GINIP-DTR and TAFA4-KO mice than for control littermates, whereas DN and MHC-II$^+$ subsets were unaffected (**Extended data Fig. 8i-l**). Thus, following exposure to UV, GINIP-DTR and TAFA4-KO mice present an imbalanced Mϕ response, with impaired survival of IL-10-producing Tim4$^+$ Mϕ and larger numbers of Inflam Mϕ. TAFA4 deficiency therefore affects both the maintenance of dermal Tim4$^+$ Mϕ and their IL-10 production capacity.

Intradermal injections of IL-10-blocking antibodies before UV irradiation in WT mice induced a phenotype similar to that of *Tafa4*-KO mice (Extended data **Fig. 9a-c**), suggesting that IL-10 upregulation is essential for Tim4$^+$ Mϕ maintenance. Similarly, IL-10-deficient mice (*Il-10$^{gfp/gfp}$* mice) exposed to UV had smaller numbers of Tim4$^+$ Mϕ, larger numbers of Inflam Mϕ, and greater skin damage (**Extended data Fig. 9d-f**). IL-10 defects are, therefore, sufficient to mimic the phenotype of GINIP-DTR and *Tafa4*-KO mice, suggesting that IL-10 acts downstream from TAFA4 signaling.

Consistent with the crucial role of IL-10-producing Mϕ in this model, we found that resident Mϕ depletion by CSF-1R-blocking antibody (AFS98)[17] treatment before UV exposure decreased total skin IL-10 content (**Extended data Fig. 9g-j**). Monocyte infiltration after resident Mϕ depletion led to the rapid reconstitution of MHC-II$^+$ and

DN Mϕ subsets, whereas Tim4^{+} Mϕ generation took up to six days (**Extended data Fig. 9k**). Mϕ-depleted mice presented increases in the number of Inflam Mϕ and skin damage pi (**Extended data Fig. 9l-n**), demonstrating the requirement of a TAFA4/dermal resident Mϕ axis for regulating Inflam Mϕ responses. Furthermore, adoptive transfer of sorted dermal Tim4^{+} Mϕ in the skin of GINIP-DTR mice pi was sufficient to limit tissue damage (**Extended data Fig. 10a-d**). Thus, the early loss of dermal resident Tim4^{+} Mϕ determines the tissue damage and repair defect rates in GINIP-DTR and TAFA4-KO mice.

Finally, the phenotype of TAFA4-KO mice was rescued by intradermal injections of recombinant TAFA4 pi (**Fig. 4g, h**). TAFA4 administration was also sufficient to upregulate Tim4^{+} Mϕ IL-10 production in TAFA4-KO mice (Extended data **Fig. 10e-f**). These data suggest that TAFA4 production by C-LTMR nerve endings after UV exposure is necessary and sufficient to downregulate inflammatory processes by modulating dermal Mϕ homeostasis and IL-10 production.

Discussion

This study reveals a crucial immunoregulatory role of non-peptidergic GINIP^{+} cutaneous sensory neurons in tissue repair, through TAFA4 production, promoting early and persistent IL-10 production by dermal macrophages. TAFA4 ensures the survival of embryo-derived Tim4^{+} Mϕ and sustains their production of large amounts of IL-10. This neuro-immune pathway downregulates Inflam Mϕ expansion, thereby reducing inflammatory cytokine levels, and promoting skin repair (**Extended data Fig. 10g**). These data are consistent with the metabolic reprograming capacity of IL-10[29] and with previous reports of IL-10 deficiency leading to excessive collagen deposition during wound healing[30]. The regulatory role of TAFA4 is not limited to Tim4^{+} Mϕ.

TAFA4 can also modulate the inflammatory profile of other macrophage subsets *in vitro* and *in vivo,* including other $CD206^+$ dermal Mϕ subsets and peritoneal Mϕ.

Recent studies of genetic or chemical ablations of sensory neuron subsets have revealed a regulatory role of the somatosensory nervous system in cutaneous immune responses[3,5-9], which may be pro- or anti-inflammatory. The considerable functional and phenotypic heterogeneity of somatosensory neurons[31-33], and their selective or combinatorial stimulation, may account for immunoregulatory differences between pathological contexts. Previous studies have identified an important role of $TRPV1^+$ neurons and the neuropeptide CGRP in bacterial and fungal infections and models of sterile and imiquimod-induced cutaneous inflammation[3,5-7,9]. Our study reveals a crucial immunomodulatory role of TAFA4 production by C-LTMRs in a sunburn-like model of skin damage. By contrast, no such effect was observed in a model of imiquimod-induced skin inflammation (**Extended data Fig. 10h**). It will therefore be important to determine whether this novel neuroimmune regulatory pathway also plays a role in the skin in other pathological contexts. The properties of TAFA4 could be exploited therapeutically to modulate inflammation in other inflammatory diseases or in patients with wound healing defects.

References

1 Wynn, T. A. & Vannella, K. M. Macrophages in Tissue Repair, Regeneration, and Fibrosis. *Immunity* **44**, 450-462, doi:10.1016/j.immuni.2016.02.015 (2016).

2 Merad, M. *et al.* Langerhans cells renew in the skin throughout life under steady-state conditions. *Nat Immunol* **3**, 1135-1141, doi:10.1038/ni852 (2002).

3 La Russa, F. *et al.* Disruption of the Sensory System Affects Sterile Cutaneous Inflammation In Vivo. *J Invest Dermatol* **139**, 1936-1945 e1933, doi:10.1016/j.jid.2019.01.037 (2019).

4 Lopes, D. M. & McMahon, S. B. Ultraviolet Radiation on the Skin: A Painful Experience? *CNS Neurosci Ther* **22**, 118-126, doi:10.1111/cns.12444 (2016).

5 Chiu, I. M. *et al.* Bacteria activate sensory neurons that modulate pain and inflammation. *Nature* **501**, 52-57, doi:10.1038/nature12479 (2013).

6 Riol-Blanco, L. *et al.* Nociceptive sensory neurons drive interleukin-23-mediated psoriasiform skin inflammation. *Nature* **510**, 157-161, doi:10.1038/nature13199 (2014).

7 Kashem, S. W. *et al.* Nociceptive Sensory Fibers Drive Interleukin-23 Production from CD301b+ Dermal Dendritic Cells and Drive Protective Cutaneous Immunity. *Immunity* **43**, 515-526, doi:10.1016/j.immuni.2015.08.016 (2015).

8 Pinho-Ribeiro, F. A. *et al.* Blocking Neuronal Signaling to Immune Cells Treats Streptococcal Invasive Infection. *Cell* **173**, 1083-1097 e1022, doi:10.1016/j.cell.2018.04.006 (2018).

9 Cohen, J. A. *et al.* Cutaneous TRPV1(+) Neurons Trigger Protective Innate Type 17 Anticipatory Immunity. *Cell* **178**, 919-932 e914, doi:10.1016/j.cell.2019.06.022 (2019).

10 Gaillard, S. *et al.* GINIP, a Galphai-interacting protein, functions as a key modulator of peripheral GABAB receptor-mediated analgesia. *Neuron* **84**, 123-136, doi:10.1016/j.neuron.2014.08.056 (2014).

11 Basbaum, A. I., Bautista, D. M., Scherrer, G. & Julius, D. Cellular and molecular mechanisms of pain. *Cell* **139**, 267-284, doi:10.1016/j.cell.2009.09.028 (2009).

12 Abraira, V. E. & Ginty, D. D. The sensory neurons of touch. *Neuron* **79**, 618-639, doi:10.1016/j.neuron.2013.07.051 (2013).

13 Abrahamsen, B. *et al.* The cell and molecular basis of mechanical, cold, and inflammatory pain. *Science* **321**, 702-705, doi:10.1126/science.1156916 (2008).

14 Braz, J. M. & Basbaum, A. I. Differential ATF3 expression in dorsal root ganglion neurons reveals the profile of primary afferents engaged by diverse noxious chemical stimuli. *Pain* **150**, 290-301, doi:10.1016/j.pain.2010.05.005 (2010).

15 Urien, L. *et al.* Genetic ablation of GINIP-expressing primary sensory neurons strongly impairs Formalin-evoked pain. *Sci Rep* **7**, 43493, doi:10.1038/srep43493 (2017).

16 Gomez Perdiguero, E. *et al.* Tissue-resident macrophages originate from yolk-sac-derived erythro-myeloid progenitors. *Nature* **518**, 547-551, doi:10.1038/nature13989 (2015).

17 Hoeffel, G. *et al.* C-Myb(+) erythro-myeloid progenitor-derived fetal monocytes give rise to adult tissue-resident macrophages. *Immunity* **42**, 665-678, doi:10.1016/j.immuni.2015.03.011 (2015).

18 Hoeffel, G. & Ginhoux, F. Fetal monocytes and the origins of tissue-resident macrophages. *Cell Immunol* **330**, 5-15, doi:10.1016/j.cellimm.2018.01.001 (2018).

19 Ginhoux, F. & Jung, S. Monocytes and macrophages: developmental pathways and tissue homeostasis. *Nat Rev Immunol* **14**, 392-404, doi:10.1038/nri3671 (2014).

20 Guilliams, M., Mildner, A. & Yona, S. Developmental and Functional Heterogeneity of Monocytes. *Immunity* **49**, 595-613, doi:10.1016/j.immuni.2018.10.005 (2018).

21 Li, L. *et al.* The functional organization of cutaneous low-threshold mechanosensory neurons. *Cell* **147**, 1615-1627, doi:10.1016/j.cell.2011.11.027 (2011).

22 Delfini, M. C. *et al.* TAFA4, a chemokine-like protein, modulates injury-induced mechanical and chemical pain hypersensitivity in mice. *Cell Rep* **5**, 378-388, doi:10.1016/j.celrep.2013.09.013 (2013).
23 Reynders, A. *et al.* Transcriptional Profiling of Cutaneous MRGPRD Free Nerve Endings and C-LTMRs. *Cell Rep* **10**, 1007-1019, doi:10.1016/j.celrep.2015.01.022 (2015).
24 Tom Tang, Y. *et al.* TAFA: a novel secreted family with conserved cysteine residues and restricted expression in the brain. *Genomics* **83**, 727-734, doi:10.1016/j.ygeno.2003.10.006 (2004).
25 Wang, W. *et al.* FAM19A4 is a novel cytokine ligand of formyl peptide receptor 1 (FPR1) and is able to promote the migration and phagocytosis of macrophages. *Cell Mol Immunol* **12**, 615-624, doi:10.1038/cmi.2014.61 (2015).
26 Grimbaldeston, M. A., Nakae, S., Kalesnikoff, J., Tsai, M. & Galli, S. J. Mast cell-derived interleukin 10 limits skin pathology in contact dermatitis and chronic irradiation with ultraviolet B. *Nat Immunol* **8**, 1095-1104, doi:10.1038/ni1503 (2007).
27 Yona, S. *et al.* Fate mapping reveals origins and dynamics of monocytes and tissue macrophages under homeostasis. *Immunity* **38**, 79-91, doi:10.1016/j.immuni.2012.12.001 (2013).
28 Hoeffel, G. *et al.* Adult Langerhans cells derive predominantly from embryonic fetal liver monocytes with a minor contribution of yolk sac-derived macrophages. *J Exp Med* **209**, 1167-1181, doi:10.1084/jem.20120340 (2012).
29 Ip, W. K. E., Hoshi, N., Shouval, D. S., Snapper, S. & Medzhitov, R. Anti-inflammatory effect of IL-10 mediated by metabolic reprogramming of macrophages. *Science* **356**, 513-519, doi:10.1126/science.aal3535 (2017).
30 Eming, S. A. *et al.* Accelerated wound closure in mice deficient for interleukin-10. *Am J Pathol* **170**, 188-202, doi:10.2353/ajpath.2007.060370 (2007).
31 Cavanaugh, D. J. *et al.* Distinct subsets of unmyelinated primary sensory fibers mediate behavioral responses to noxious thermal and mechanical stimuli. *Proc Natl Acad Sci U S A* **106**, 9075-9080, doi:10.1073/pnas.0901507106 (2009).
32 Usoskin, D. *et al.* Unbiased classification of sensory neuron types by large-scale single-cell RNA sequencing. *Nat Neurosci* **18**, 145-153, doi:10.1038/nn.3881 (2015).
33 Sharma, N. *et al.* The emergence of transcriptional identity in somatosensory neurons. *Nature* **577**, 392-398, doi:10.1038/s41586-019-1900-1 (2020).

411 **Figure legends**

412 **Figure 1: GINIP$^+$ sensory neurons prevent fibrosis after UV exposure**

413 **a**, Experimental scheme indicating the phases of skin inflammation, resolution and
414 repair after overexposure to UV radiation (See also **Extended data fig. 1a** for
415 inflammatory and pro-repair gene expression pi). **b**, *Atf3* mRNA levels in C2/C3 DRGs
416 over time in UV-irradiated (purple dots) and non-exposed mice (gray dots), (*n*=5 mice
417 per group). **c**, Confocal images of GINIP (red), CGRP (blue) and ATF3 (green)
418 expression in DRGs, from unexposed (No UV) and UV-exposed mice (D3 UV). (See
419 also C2/C3 DRG characterization in **Extended data fig. 1b-f). d**, Percentage of ATF3$^+$
420 neurons from C2/C3 DRGs positive for CGRP (blue) or GINIP (red) at D3 pi (n=8 mice
421 per group). **e**, Changes in ear thickness over time pi, in control DTR (blue) and GINIP-
422 DTR mice (red), (*n*=7 mice per group). **f**, Representative control DTR (left) or GINIP-
423 DTR mice (right) ears on D14 pi. (see also neuron depletion in GINIP-DTR skin,
424 **Extended data fig. 2a-b).** Representative H&E staining of ear sections from control
425 DTR (**g**), and GINIP-DTR mice (**h**), at D35 pi. Fibrosis (**i**), and cumulative
426 histopathological score (**j**), at D35 pi (*n*=5 mice per group). (See also **Extended data**
427 **fig. 2d-j** for detailed analysis of histopathological score, scratching behavior and back
428 skin analysis). Data are presented as mean ± SEM and representative for at least two
429 independent experiments. One-way ANOVA with Tukey tests, except for **b** and **e**, two-
430 way ANOVA and **d**, Student's *t*-test.

431

432 **Figure 2: Dermal-resident Tim4$^+$ macrophage maintenance is compromised in**
433 **UV-exposed GINIP-DTR mice**

434 **a**, Confocal analysis of ear skin from Nav1.8-RFP mice stained for GINIP$^+$ neurons
435 (green) and CD206$^+$ dermal resident Mϕ (blue). **b**, Distance (μm) between CD206$^+$ Mϕ

and GINIP^{+} axons (n=97 Mϕ). (See also **Extended data Fig. 3g** for higher magnification). **c**, Cluster analysis and t-SNE distribution of Mo/Mϕ subsets. Monocyte-related subsets (CCR2^{+}) clustered as Ly6C^{+} Mo (Ly6C^{+}, orange), Int. Mo (Ly6C^{int}, MHCII^{int}, light green), PMo (Ly6C^{-}, MHCII^{-}, CD64^{-}, dark green) and their derivatives MoDC (Ly6C^{-}, MHCII^{+}, blue) and Inflam Mϕ (Ly6C^{-}, MHCII^{-}, CD64^{+}, CD206^{-}, pink). Dermal resident Mϕ (CD64^{+}CD206^{+}) subsets were identified as MHCII^{+} Mϕ (MHCII^{+}, Tim4^{-}, red), DN Mϕ (MHCII^{-}, Tim4^{-}, purple) and Tim4^{+} Mϕ (MHCII^{-}, Tim4^{+}, cyan). (See also **Extended data Fig. 3a, and 4a-c; 4e-g** for detailed gating strategy and t-SNE analysis, and **Extended data Fig. 4d-f** for subset quantification). **d**, t-SNE clustering of Mo/Mϕ subsets in DTR (left) or GINIP-DTR (right) mice at D14 pi. **e**, Absolute numbers of Tim4^{+} Mϕ (cyan) or **f**, Inflam Mϕ (pink), per mg ear skin (*n*=10-14 mice per group) from DTR (gray) or GINIP-DTR (colored) mice, between days 0 and 14 pi. Data are presented as mean ± SEM and representative for at least two independent experiments. One-way ANOVA with Tukey tests (ns: non-significant).

Figure 3: TAFA4, a neuropeptide expressed by C-LTMRs, regulates IL-10 production by macrophages and prevents UV-induced skin fibrosis

a, Representative confocal images of C3 DRGs from WT mice on day 3 (D3) pi stained with IB4 (blue), anti-TAFA4 (red) and anti-ATF3 antibodies (green). **b**, Percentage ATF3^{+} neurons positive for IB4 (blue) and TAFA4 (red) (*n*=8 mice per group). **c**, Quantification of TAFA4 protein (ELISA) in WT mice ear skin from D0 to D35 pi (*n*=6-18 mice per group). (See **Extended data Fig. 5** for C-LTMRs analysis and TAFA4 detection). **d**, Representative Picro Sirius staining of ear sections from WT (top) and *Tafa4*-KO (bottom) mice at D35 pi and **e**, collagen deposition: percentage

fibrosis (yellow pixels) over the total area (red + yellow pixels), (*n*=9 mice per group). **f**, TNFα and **g**, IL-10 protein levels (CBA) in ear skin lysates (*n*=4-8 mice per group). **h**, Relative *Il10* mRNA levels in sorted dermal $CD206^+$ Mϕ from WT (blue) and *Tafa4*-KO (red) mice between days 0 and 10 pi (pooled from 3 independent sortings, each with *n*=3 mice per group). **i**, Relative *Tnfa*, *Il1b* and *Il10* mRNA levels (RT-qPCR) for purified peritoneal Mϕ (ThioMϕ) activated *in vitro* with LPS (100 ng/ml) without (blue) or with TAFA4 (100 nM; green), (*n*=5-8 independent samples). Data are presented as means ± SEM and representative for at least two independent experiments. One-way ANOVA with Tukey tests, except for **b** and **f**, Student's *t*-test **c**, Kruskal-Wallis test, and **d**, two-way ANOVA (ns: non-significant; **p* < 0.05; ***p* < 0.01; ****p* < 0.001).

Figure 4: The TAFA4-IL-10 axis promotes Tim4$^+$ macrophage survival and tissue repair functions

a, Experimental strategy for generating CD45.1 BM chimeras in CD45.2 WT or *Tafa4*-KO recipient mice and monitoring monocyte-derived cells pi. **b**, FACS and t-SNE analysis of skin Mo/Mϕ subsets 7 days pi, as described in **Fig. 2** (See also **Extended data fig. 8f-h** for detailed BM chimera analysis). **c**, t-SNE analysis of CD45.2$^+$ and CD45.1$^+$ clusters (yellow and black) and intracellular staining for IL-1β, TNFα and IL-10 (red). **d**, Absolute numbers of Inflam Mϕ in WT control (gray) and *Tafa4*-KO BM-chimeric mice (pink). **e**, Absolute numbers of CD45.2$^+$Tim4$^+$ Mϕ (left) and percentage of CD45.1 chimerism in total Tim4$^+$ Mϕ (right) from WT (gray) and *Tafa4*-KO BM-chimeric mice (cyan). **f**, Absolute numbers of total (CD45.1$^+$ and CD45.2$^+$) Tim4$^+$ Mϕ in WT (gray) and *Tafa4*-KO BM-chimeric mice (cyan), (n=6-10 mice per group). **g**, Intradermal TAFA4 protein injection in *Tafa4*-KO mice (green arrows) and changes in ear thickness over 21 days pi in saline-treated WT (blue) and *Tafa4*-KO (red) mice, or *Tafa4*-KO mice treated with TAFA4 (green) (n=14 mice per group). **h**, Absolute numbers of Inflam Mϕ (left) and Tim4$^+$ Mϕ (right) in ear skin on day 14 pi (n=11 mice per group). Data are presented as mean ± SEM and representative for at least two independent experiments. One-way ANOVA with Tukey tests except for (**g**), two-way ANOVA (ns: non-significant; *$p < 0.05$; **$p < 0.01$; ***$p < 0.001$).

Methods

Mice

C57/Bl6J mice were bought from Janvier Labs (https://www.janvier-labs.com). GINIP-DTR mice were obtained by crossing GINIP$^{flx/+}$ line[10] with mice expressing the CRE recombinase from *Nav1.8* locus (*Nav1.8$^{Cre/Cre}$* mice)[13]. One single

diphtheria toxin (DT; 10μg/kg) injection in *Nav1.8*$^{Cre/+}$ GINIP$^{flx/+}$ (hereafter called GINIP-DTR mice) allowed the specific ablation of GINIP^{+} sensory neurons[15]. *Nav1.8*$^{+/+}$ GINIP$^{flx/+}$ littermates (hereafter called DTR mice) treated with DT were used as controls throughout. *Nav1.8*^{rfp} were obtained by crossing *Nav1.8*$^{Cre/+}$ with flxR26-RFP mice. Homozygotes *IL-10*$^{gpf/gfp}$ mice, described previously[34,35] were used with their heterozygotes IL-10$^{gfp/wt}$ control littermates. *Tafa4*-KO mice were generated in Aziz Moqrich's lab (IBDM, AMU, France) and described previously[22]. CX3CR1^{CreERT2}:R26-YFP mice were described previously[27]. All the mice used were bred and maintained under specific pathogen-free conditions at the Centre d'Immunophénomique (Ciphe) de Marseille and at the Centre d'Immunologie de Marseille Luminy (CIML). Mice were housed under a standard 12 h:12 h light-dark cycle with ad libitum access to food and water. Age-matched (6-12 weeks old, unless specified in figure legend) and sex-matched littermate mice were used as controls. All experiments were conducted in accordance with institutional committee recommendations (Comité d'Éthique de Marseille no. 14-APAFiS # 18469-2019011417196625v2) and French and European guidelines for animal care.

Bone marrow chimera generation

Age and sex matched WT or *Tafa4*-KO mice (CD45.2^{+}) were anaesthetized with ketamine/xylazine (10μl/g, 2% Imalgene500/ 5% Rompun). Mice were then irradiated with 6,5Gy from an γ-ray irradiator. A lead shield was used to protect the ear's skin from γ-irradiation. Six hours after irradiation, 30mg/kg Busulfan (Sigma)[36] was injected (i.p.) to deplete remaining myeloid progenitors in recipient mice. Twelve hours later the mice were reconstituted with 5 million CD45.1^{+} bone marrow (BM) cells. Mice were treated with Bactrim (in drinking water) for two weeks for a total recovery time of 6 weeks before analyzing the blood CD45.1 chimerism and were then used for experiments.

Lineage tracing study

CX3CR1$^{Creert2:R26R\text{-}EYFP+/+}$ were used as described[27]. Tamoxifen (2mg Tam/mice; 40mg/ml in corn oil; Sigma) was injected i.p. to pregnant mice at E16.5 days post-conception (dpc). Day of embryonic development (E) was estimated by taking the

day of vaginal plug observation as E0.5 dpc. Caesarian sections were carried out at term and neonates were fostered by lactating females. In this model, Tam-induced recombination leads to irreversible expression of the enhanced yellow fluorescent protein (EYFP) in CX3CR1^{+} embryonic precursors and their progeny (i.e. fetal monocytes and differentiated Mϕ at the time of Tam injection; for review see[37]).

UV-induced skin injury

Mice were anaesthetized with ketamine/xylazine, shaved and depilated (Veet Cream) and then left untreated or exposed to UV (λ 254nm; voltage: 8W; source: 30cm from the target) for 25 min. The protocol described previously[2] was adapted so that the ear skin of WT mice can recover in 35 days after UV exposure. Ear thickness was measured every other day with a caliper (under isoflurane anesthesia) and compared to the ear thickness of control untreated mice.

Histology and histopathological analysis

At different time pi, mice were lethally anesthetized ketamine/xylazine (20µl/g) and perfused with 10ml of PBS. Ears were then collected and fixed with formol (for at least 1h), then cryoprotected with sucrose 30% overnight and embedded in paraffin. Skin sections of 5µm were stained with hematoxylin and eosin, Masson's trichrome or picrosirius red. Histological scores were blindly assessed by a pathologist following the criteria described below. Leukocyte infiltration, epidermal thickness and fibrosis were evaluated and a score was assigned based on severity for each criterion. Fibrosis was also evaluated using a semi-quantitative binary score based on percentage of surface modified by fibrotic changes. A cumulative score was then obtained.

Histopathological grading

Inflammation/leukocyte infiltration

(0): No inflammation; (1): Mild dermatitis (less than 10 leukocytes per High Power Fields, HPF); (2): Moderate dermatitis (less than 50 leukocytes/HPF); (3): Marked dermatitis (less than 100 leukocytes/HPF); (4): Severe dermatitis (more than 100 leukocytes/HPF).

Epidermal thickness

(0): Normal thickness; (1): Mild hyperplasia (less than 4 cellular layers); (2): Moderate hyperplasia (more than 4 cellular layers); (3): Marked hyperplasia (markedly thickened, stratification and epidermal crest)

Wound healing/fibrosis

(0): No granulation tissue, no fibrosis; (1): Early granulation tissue and mild fibrosis; (2): Moderate fibrosis (hair follicle obliteration); (3): Marked fibrosis (persistent granulation tissue/cartilage obliteration)

Fibrosis extension

(1): Focal or multifocal fibrosis (less than 50% fibrosis per HPF); (2): Extensive fibrosis (more than 50% fibrosis per HPF)

Dorsal Root Ganglia (DRG) tissue sections

After lethal anesthesia and perfusion with 5 ml of PBS and 25 ml of 4% paraformaldehyde (PFA), C2/C3 DRG were carefully dissected from the spinal cord under a binocular lens, fixed for 1 hour with 4% PFA and then cryoprotected with 30% (w/v) sucrose overnight before being included in OCT (Tissue-Tek, Sakura) and stored at -80°C. DRG samples were sectioned at 10µm using a standard cryostat (Leica).

In situ Hybridization on DRG

In situ hybridization was carried out following the protocol described in[15]. Briefly, RNA probes were synthesized using gene-specific PCR primers and cDNA templates from mouse DRG. The following oligonucleotides were used for the nested PCRs for probe synthesis:

Tafa4-F1: TGCTCAGAAGTTCATAGCCAAA

Tafa4-R1: TAAAGGAACATTTGCAAGCTCA

Tafa4-F2: ATATGTGCAGTGTGG

Tafa4-R2 + T7: TAATACGACTCACTATAGGGCAGCCAAGTTCAAAC

DRG sections were treated with proteinase K, triethanolamine and acetic anhydride solutions. Digoxigenin labeled probes were hybridized overnight at 55°C after 2h of prehybridization. The slides were treated with 0.2X SSC baths

then blocked at room temperature with 10% Goat serum and incubated with anti-digoxigenin antibodies (Roche). Final detection was achieved using Cyanine 3 TSA plus kit (Perkin Elmer).

Immunofluorescent and confocal analysis of DRG neuron activation

We used the expression of ATF3 (Activating Transcription Factor 3) as a proxy for neuronal injury and activation[38]. DRG sections were saturated and permeabilized with a PBS 1X, 3% BSA, 0,3% Triton 100X and 10% Donkey serum (Sigma; #D9663-10ML) solution for 1 hour at room temperature (RT) before adding the primary anti-mouse TAFA4 antibody (rat clone 1D8, 1:1000), the anti-mouse GINIP (rat, 1:1000, Aziz Moqrich's lab, IBDM) or the anti-mouse GINIP (rabbit, 1:1000, Invitrogen #PA5-71131), the anti-mouse ATF3 (rabbit, 1:200, Santa Cruz #SC-188 or Abcam #ab207434), the anti-TH (1:300, Merck Millipore, #AB152) and anti-mouse CGRP (goat, 1:1000, Abcam #ab36001) for 24 hours at 4°C. After several washes, donkey secondary antibodies (anti-mouse, #715-585-151; anti-rat, #712-545-153; anti-rabbit, #711-585-152; and anti-goat, #705-605-147; from Jackson ImmunoResearch, 1:500) were added for 45 minutes at room temperature. The staining with the lectin isolectin B4 (IB4) coupled to AlexaFluor 647 (AF647; 1:200, Invitrogen) was performed in TNT buffer (Tris HCl 100 nM, NaCl 150 nM, Tween-20 0,1% pH 7,5) for 45 minutes at room temperature. Images were acquired using a confocal microscope LSM780 (Zeiss) and analyzed using ZEN 2.3 and ImageJ Software.

Skin cell isolation

After lethal anesthesia and intracardiac perfusion with 5 ml of PBS, ears were collected and dorsal and ventral layer separated, finely minced with scissor in complete medium (RPMI+L-Glutamine, 10% FCS) and incubated 1h at 37°C with 1mg/ml DNase (Roche) 0.2mg/ml Dispase (GIBCO) and 0.2mg/ml collagenase type IV (Sigma; #C5138-500MG). Tissues were then dissociated using 2.5 ml syringes and 18G needles and filtered on cell strainer (100 μm, BD), washed in FACS buffer (PBS-2mM EDTA, FCS 2%) to obtain a homogeneous cell suspension ready for staining.

DRG neurons isolation

After lethal anesthesia and intracardiac perfusion with 5 ml of HBSS 10X (Mg^- Ca^{2-}), HEPES 5 mM, D-Glucose 12.5 mM, and penicillin/streptomycin (P/S) 1% solution, DRGs were carefully extracted and digested twice with a 0.2 mg/ml collagenase type II (Gibco), and 0.5 mg/ml dispase (Gibco) solution for 30 minutes at 37°C. After several wash with Neurobasal complete medium (B-27 2%, L-glutamine 20 mM, P/S 1%), DRGs were mechanically dissociated using 3 needles of decreasing diameter (18G, 22G, 26G). After a filtration on a cell strainer (70 μm, Miltenyi Biotec), a Percoll gradient was used with 12.8% and 28% density in Leibovitz-15 complete medium (FCS 5% and P/S 1%) to eliminate cell debris. After centrifugation and several washes, the cell suspension was ready for staining.

Antibodies for flow cytometry

We adapted our FACS gating strategy from previous studies[39], adding EpCAM, Langerin (CD207) or CD206 and Tim4 to decipher the Mo/Mϕ compartment of the skin. Antibodies were purchased from BioLegend or BD Biosciences: CD45-BV785 1:500 (30F11), CD45.1-BV605 1:200 (A20), CD11b-BV510 1:1000 (M1/70), CD64-BV711 1:300 (X54-5/7.1), Ly6C-421 1:300 (AL-21), F4/80-PECF594 1:400 (T45-2342), CD11c-BUV395 1:200 (N418), EpCAM-AF594 1:500 (G8.8), CD207-APC (929F3.01; Dendritics, #DDX0362), CD206-APC 1:300 (C068C2), Tim4-PeCy7 (RMT4-54) Ly6G-APC-Cy7 1:300 (1A8), IA-IE A700 1:500 (M5/114.15.2), CD24-BUV737 1:500 (M1/69). Mast cells were characterized as previously described[40,41], CD117-BV605 (c-kit; 2B8; 1:300), CD103-PerCP-Cy5.5 (2E7; 1:500), anti-TNFα-PE 1:100 (MP6-XT22) anti-IL-10-PE 1:100 (JES5-16E3); CCR2-PE 1:200 (475301; R&D System), IL-1β-PE Ab 1:100 (NJTEN3; eBioscience), anti-CD4 PE-Cy7 (RM4-5; BD), anti-TCRαβ APC-Cy7 (H57-597; BD), anti-FoxP3-A488 1:200 (Clone FJK-16s; eBioscience), anti-DTR 1:300 (anti-hHB-EGF; AF-259-NA; R&D System), anti-GFP (Invitrogen, #A-21311).

Flow cytometry

Cell suspensions were plated in 96 well U bottom plates and stained at 4°C. Cells were incubated 40min at 4°C in FACS buffer with antibodies and anti-Fc receptor

blocking antibody (clone: 2.4 G2). Cells were then washed and fixed (fixation buffer, from FoxP3 kit; eBioscience; #00-5521-00) until analysis. For intra-cellular cytokine staining, cell suspensions were permeabilized (Fix/perm, from FoxP3 kit; eBioscience) and stained with anti-cytokine antibodies during 1h for IL-1β and TNFα or overnight for IL-10. For IL-10 expression analysis in FoxP3$^+$ Treg cells, total skin homogenates were incubated during 6h in complete medium supplemented with PMA (200ng/ml; Sigma) and ionomycin (1mg/ml; Sigma). During the last 4h, Golgi Plug (1:1000; BD Biosciences; #554724) was added. Cell suspensions were then washed extensively at 4^{o}C, surface stained, fixed and then processed for intracellular staining. Dead cells were excluded from the analysis by counter-gating using the live/dead fixable blue Dead Cell Stain kit UV (L23105; Invitrogen). Multiparameter FACS analysis was performed using an LSR X20 system (BD). Absolute numbers for each population were obtained using Quanti Beads (BD Biosciences, #556296). Data analysis was performed using Flowjo software (Tree Star, Inc.).

t-distributed Stochastic Neighbor Embedding (t-SNE)

t-SNE analyses were performed with FlowJo™ version 10 software (FlowJo LLC). We used an equal number of mice for each genotype or experimental condition considered. In each group, the same number of cells was used to allow an equivalent contribution of each individual mice in the analysis. This equal cell number was selected using the DownSample plugin. Then, cells from each mouse were merged using the concatenate tool and barcoded to track and distinguish them. Finally, t-SNE analyses were performed using different markers, indicated in the figure legends. The color code representing the expression level of each marker in the heatmaps (depicted in extended data figures), is normalized on the median intensity value for a given marker. Data are represented using a four-color scale with blue, green-yellow and red indicating respectively low intermediate and high expression levels.

Immunofluorescent staining and confocal microscopy analysis of ear skin

After lethal anesthesia and perfusion with 10ml PBS, ears from DT-treated GINIP-DTR and -DTR control mice were collected and ear dorsal and ventral layers were

separated, fixed for 1 hour with 4% PFA, washed, permeabilized and saturated with a PBS, 3% BSA, 0,2% Triton 100X and 10% donkey serum and then stained with the primary anti-mouse GINIP antibody (rat, 1:1000, Aziz Moqrich's lab, IBDM) , the anti-TH antibody (rabbit,1:300; Merck Millipore, #AB152) overnight at 4°C. After several washes, a donkey secondary anti-rat-488 and anti-rabbit-AF594 antibody (Jackson Immunoresearch, 1:500) were added 1h at 4°C, washed, and then the anti-Beta III Tubulin-AF647 antibody (1:300 TUJI; Biolegend, #BLE801210) or the anti-CD206-APC 1:300 (rat, 1:300; clone C068C2, Biolegend, #BLE141708), were added for additional 45 minutes at room temperature. After several washes slices were then mounted on coverslips with mounting medium and image acquisition was performed on Confocal LSM780 (Zeiss) and analyzed with ZEN and ImageJ software.

Bone marrow-derived macrophage (BMDM) generation

Femora bones were isolated from WT or FPR1-KO mice (We thank Pr Monica Lucattelli and Pr Laurence Zitvogel for providing BM cells from FPR1-KO mice), cut in half and placed in 0.5ml Eppendorf tubes pre-perforated on their bottom part. The small tubes with two ½ bone were placed within 1.5ml Eppendorf tubes. The tubes were then centrifuged 10sec at 10000rpm and BM cell pellets were resuspended in red blood cell lysis buffer for 3 minutes and washed in PBS. BM cells were then resuspended at 10^6/ml in complete DMEM (DMEM, SVF 10%, P/S, 1% L-Glu) supplemented with 20% conditioned L929 media during 5 days to generate bone marrow derived-macrophages (BMDM) and used as ThioMϕ for *in vitro* experiments.

Thioglycollate-elicited macrophage (ThioMϕ) generation and in vitro treatment

Peritoneal macrophages were isolated from WT mice by peritoneal wash three days after 3% Thioglycollate (Sigma) i.p. injection. Peritoneal washes were then stained with biotin-associated lineage cocktail antibodies (CD3, CD19, NK1.1, Ly6G and Siglec F), counterstained with anti-biotin microbeads (Miltenyi Biotec) and then purified using magnetic LS columns. Peritoneal macrophage preparations were then cultured in complete DMEM (DMEM, SVF 10%, P/S, 1% L-Glu) at 10^6 ThioMϕ/ml in a 12-well plates (BD) with or without LPS (100ng.ml,

Sigma) in the presence of not of 100nM TAFA4. After 16 hours, macrophages were lysed using RLT medium (Qiagen) then pass through a QIAShredder column (Qiagen) and store at -80°C.

Migration assay

BMDM from WT or FPR1-KO mice were incubated on the top chambers of transwell plates (Costar) in complete DMEM, while the bottom chambers of the transwell plates were filled with complete DMEM for negative control, or complete DMEM containing CCL2 (MCP-1; 10nM) for positive control of migration, or increasing concentrations of TAFA4 (1 to 1000nM), during 8h at 37°C. The bottom chambers were then analyzed by FACS for macrophages content.

Dermal resident macrophage depletion.

WT or *Tafa4*-KO mice were injected two consecutive days with 500µg of the CSF-1R blocking antibody (clone AFS98; *InVivo*MAb, BioXcell #BE0213) or the isotype control (IgG2a; clone 2A3; *InVivo*MAb, BioXcell #BE0089). One day after the last injection, mice tissues were collected and analyzed for Macrophage depletion by flow cytometry.

Dermal resident macrophage isolation

Ears skin from WT or *Tafa4*-KO mice were dissociated and stained as previously described, and $CD206^+$ dermal resident macrophages were cell sorted on a FACS Aria III following the Figure 2 gating strategy as $livedead^{neg}$, $CD45^+$ DC^{neg} $CD11b^+CD24^-Ly6G^-CCR2^-Ly6C^-CD64^+CD206^+$, then lysed using RLT medium (Qiagen) then pass through a QIAShredder column (Qiagen) and store at -80°C. Alternatively, $Tim4^+$ Mϕ or Inflam Mϕ ($CD64^+CD206^-$) were sorted as presented in Extended data Figure 10b.

Intradermal adoptive transfer of Inflam and Tim4⁺ macrophages.

DTR and GINIP-DTR mice were exposed to UV and then intradermally injected at D1 pi with 2000 Mϕ/10µl PBS per ears.

Imiquimod-induced cutaneous damage.

762 Mice (WT or *Tafa4*-KO mice) were daily treated with 5mg of 5% imiquimod cream
763 (IMQ) applied topically to dorsal and ventral aspects of ear skin as describe[6],
764 during six days and evolution of the ear thickness (μm) was followed every day
765 with a caliper.
766
767 *TAFA4 rescue and in vivo blocking of IL-10*
768 For TAFA4 rescue experiments, 20 μl of recombinant TAFA4 (25 μg/ml) or saline
769 solution only, were intradermally injected every other day following the UV-
770 treatment until day 8 pi in each ear of *Tafa4*-KO or control mice as indicated in
771 figures.
772 For IL-10 blocking experiments, 20 μl of anti-IL-10 blocking antibody (0.5 mg/ml;
773 R&D, #MAB417) or the isotype control (rat IgG1; clone JES052A5) were
774 intradermally injected every other day following the UV-treatment until day 8 pi
775 in each ear of *Tafa4*-KO or control mice as indicated in figures.
776
777 *Gene expression analysis*
778 Total RNA was isolated from mouse ears, exposed or not to UV irradiation or from
779 BMDM or ThioMϕ activated with or without LPS and TAFA4. Ears were
780 dilacerated by FastPrep-24 (MpBio) in lysis matrix A tubes (MpBio). RNA was
781 isolated using a fibrous RNeasy minikit (QIAGEN). Reverse transcription was
782 performed using Superscript RTII (Invitrogen). Preamplification was performed
783 using specific Taqman probes (Applied Biosystems) for each targeted gene using
784 the pre-amplification master mix (Fluidigm). Pre-amplified products (18 cycles)
785 were diluted (1:5) in Universal PCR Master Mix then loaded in a 96.96 Dynamic
786 Array and analyzed on a BioMark Genetic Analysis System (Fluidigm). Data were
787 normalized ($2^{-\Delta Ct}$) to the housekeeping genes, *Gapdh* and *Hprt*.
788
789 *Primers used for mRNA detection in total skin samples* (*TaqMan references)*
790
791 *Acta2* (Mn00808218_g1); *Areg (*Mm00437583_m1); *Ccl1* (Mm00441236_m1);
792 Ccl2 (Mm00441242_m1); *Ccl3* (Mm00441259_g1); *Clc4*(Mm00443111_m1); *Clc6*
793 (Mm01302419_m1); *Ccl8 (*Mm01297183_m1); *Cd36* (Mm00432403_m1);
794 *Cebpb/d* (Mm00786711_s1); *Chil3* (Mm00657889_mH); *Col1a1*
795 (Mm00801666_g1); *Col3a1* (Mm00802305_g1); *Cxcl2* (Mm00436450_m1); *Cxcl9*
796 (Mm00434946_m1); *Cxcl10* (Mm00445235_m1); *Des* (Mm00802455_m1); *Egr1*

(Mm00656724_m1); *Epas* (Mm01236112_m1); *Fam19a4* (*Tafa4*, Mm00623620_m1); *Flt3* (Mm00439016_m1); *Gf1r* (Mm00616224_m1); *Ifnb1* (Mm00439552_s1); *Il1b* (Mm00434228_m1); *Il1r1* (Mm00434237_m1); *Il4* (Mm00445259_m1); *Il12a* (Mm00434169_m1); *Il13* (Mm00434204_m1); *Il15* (Mm00434210_m1); *Il17a* (Mm00439618_m1); *Il22* (Mm01226722_g1); *Il23a* (Mm00518984_m1); *Irf3* (Mm01203177_m1); *Irf7* (Mm00516791_g1); *Irf8* (Mm00492567_m1); *Klf2* (Mm00500486_g1); *Klf4* (Mm00516104_m1); *Klf5* (Mm00456521_m1); *Mmp2* (Mm00439498_m1); *Mmp9* (Mm00442991_m1); *Mmp10* (Mm01168399_m1); *Mmp12* (Mm00500554_m1); *Mpo* (Mm00447885_m1); *Mtor* (Mm00444968_m); *Nos2* (Mm00440502_m1); *Nr4a1* (Mm01300401_m1); *Nr4a3* (Mm00450071_g1); *Pdgfra* (Mm00440701_m1); *Pdgfrb* (Mm01262485_m1); *Piezo1* (Mm01241544_g1); *Piezo2* (Mm01262422_g1); *Plod2* (Mm00478767_m1); *Pparg* (Mm00440940_m1); *Retlna* (Mm00445109_m1); *Ripk1* (Mm00436360_m1); *Serpinb9* (Mm00777163_m1); *Tac1* (Mm01166994_g1); *Tgfrb2* (Mm03024091_m1); *Tlr3* (Mm01207402_m1); *Tlr4* (Mm00445273_m1); *Tlr7* (Mm04933178_g1); *Tlr9* (Mm07299609_m1); *Tp53* (Rn00755717_m1); *Gapdh* (Mm99999915_g1); *Hprt* (Mm03024075_m1).

Protein extraction from tissue

Mice were euthanized and their ears were snap-frozen in liquid nitrogen and then transferred into mechanical dissociation tubes (Lysis Matrix A, MPbio) containing a commercial lysis buffer (T-Per Tissue Protein Extraction Reagent, Thermofisher) with protease inhibitor cocktail (Halt Protease Inhibitor 100X, Thermofisher). Proteins extraction was performed by incubating each gram of tissue with 20 ml of lysis buffer. Tissues were dissociated using a 3 cycles program of FastPrep-24 5G (MPbio). After two centrifugations at 16 000 g for 30 minutes, the supernatants were filtered (on 70 µm cell strainers, Startedt) and stored at -80°C until use.

Generation of recombinant mouse TAFA4

Mouse TAFA4 recombinant protein was produced in *E. coli* by Pure Biologics (https://purebiologics.pl). The endotoxin levels of the purified protein, measured by the LAL (Limulus Amoebocyte Lysate) method, was <0.0005 EU/µg. The recombinant protein included a Histidine (His)-Tag in the C-Terminal part of the protein allowing its detection by anti-His antibodies. The sequence of this recombinant mTAFA4 is:

MHLIKPGTCEVVAVHRCCNKNRIEERSQTVKCSCFPGQVAGTTRAQPSCVEAAIV
IEKWWCHMNPCLEGEDCKVLPDSSGWSCSSGNKVKTTKVTRGGGSGLEHHHHHH

Generation of anti-TAFA4 monoclonal antibodies

Anti-TAFA4 monoclonal antibodies (mAbs) were generated by MImAbs (https://www.mimabs.org). Briefly, three Wistar rats were immunized with the recombinant mouse TAFA4 protein (100µg, 3 IP injections followed by a final boost). After immunization, spleen cells were harvested and fused to the myeloma cell line X63-Ag8-656. Hybridoma were seeded in methylcellulose semi-solid medium with CloneDetect agent (Molecular Devices #K8240) and secreting monoclonal IgG hybridomas were picked by ClonePix2 (Molecular Devices) to liquid medium 96 wells plates. Hybridoma clones producing anti-TAFA4 antibodies were selected using an ELISA screen. The specificity of the antibodies for the native TAFA4 protein was assessed by immunofluorescent staining on mouse DRG from WT (positive control) or *Tafa4*-KO (negative control) mice.

Sandwich ELISA for TAFA4 quantification

To quantify TAFA4 protein, sandwich enzyme-linked immunosorbent assay (ELISA) has been developed by MImAbs (https://www.mimabs.org). Briefly, anti-TAFA4 antibodies (clone 33F8, 50 µl, 2µg/ml) diluted in a Na_2CO_3/$NaHCO_3$ buffer (Sigma, #C3041-100CAP, pH = 9.6) were coated on 96 well MAXISORP plates (Sigma #M5785-1CS) and incubated overnight at 4°C. Plates were then washed 3 times in a washing buffer (PBS/0.1% Tween-20) and blocked with in 300 µl of StartingBlock blocking buffer (Thermofisher, #37542). Samples and serial dilutions of mTAFA4 (to establish the standard curve) were incubated 1.30 h at room temperature (RT). After 3 wash, anti-TAFA4 biotinylated antibodies (clone 1D8, 50 µl, 2µg/ml) were incubated for 1.30 h at RT. After 3 wash, HRP-Conjugated Streptavidin (Thermofisher, #N100) was added, washed 3 times before adding the substrate solution TMB (Interchim, #UP664781). After 10 additional minutes, the reaction was stopped with a solution of HCl (1M) and the absorbances (at 450 nm and 620 nm) of each well were measured. The specific signal obtained for WT ear skin samples was determined by subtracting the background signal obtained with skin samples from *Tafa4*-KO mice.

Cytokine and chemokine quantification in skin samples

Ear skin samples were homogenized and proteins extraction was performed as described above. Cytometric Bead Array (CBA) Flex Set kit (BD Bioscience) was used to quantify chemokine ligand 1 (CXCL1), tumor necrosis factor-alpha (TNFα), interleukin 6 (IL-6), interleukin 1 beta (IL-1β), monocyte chemoattractant protein 1 (CCL2/MCP1) and the chemokine (C-C motif) ligands 4 (CCL4). For IL-10, an enhanced sensitivity Cytometric Bead Array (CBA) Flex Set kit (BD Bioscience) was used. Samples were analyzed on a Canto II flow cytometer with FCAP Array TM Software (BD Bioscience) following manufacturer's instructions.

Statistical analysis

All the results are expressed as mean +/- SEM. Statistical analysis were performed using the GraphPad Prism for Windows software. Statistical analysis was performed using a one-way ANOVA with Tukey's multiple comparisons test throughout the study. A two-way ANOVA test was used to compare two or more than two groups in kinetic experiments after UV exposure, involving repeated measures on the same animals over time. Difference were considered significant as following: *$p<0.05$; **$p<0.01$; ***$p<0.001$; and ****$p<0.0001$.

Additional references:

34 Madan, R. *et al.* Nonredundant roles for B cell-derived IL-10 in immune counter-regulation. *J Immunol* **183**, 2312-2320, doi:10.4049/jimmunol.0900185 (2009).

35 Reber, L. L. *et al.* Imaging protective mast cells in living mice during severe contact hypersensitivity. *JCI Insight* **2**, doi:10.1172/jci.insight.92900 (2017).

36 Misharin, A. V. *et al.* Monocyte-derived alveolar macrophages drive lung fibrosis and persist in the lung over the life span. *J Exp Med* **214**, 2387-2404, doi:10.1084/jem.20162152 (2017).

37 Hoeffel, G. & Ginhoux, F. Ontogeny of Tissue-Resident Macrophages. *Front Immunol* **6**, 486, doi:10.3389/fimmu.2015.00486 (2015).

38 Renthal, W. *et al.* Transcriptional Reprogramming of Distinct Peripheral Sensory Neuron Subtypes after Axonal Injury. *Neuron* **108**, 128-144 e129, doi:10.1016/j.neuron.2020.07.026 (2020).

39 Tamoutounour, S. *et al.* Origins and functional specialization of macrophages and of conventional and monocyte-derived dendritic cells in mouse skin. *Immunity* **39**, 925-938, doi:10.1016/j.immuni.2013.10.004 (2013).

40 Gentek, R. *et al.* Hemogenic Endothelial Fate Mapping Reveals Dual Developmental Origin of Mast Cells. *Immunity* **48**, 1160-1171 e1165, doi:10.1016/j.immuni.2018.04.025 (2018).

41 Serhan, N. *et al.* House dust mites activate nociceptor-mast cell clusters to drive type 2 skin inflammation. *Nat Immunol* **20**, 1435-1443, doi:10.1038/s41590-019-0493-z (2019).

Acknowledgments

We thank Vincent Feuillet for critical reading of the manuscript and for helpful comments and discussions. We thank Justine Galluso for mouse breeding and genotyping. We thank the Centre d'Immunologie de Marseille-Luminy (CIML) mouse house and core cytometry, imaging and histology facilities. The S. U. laboratory received funding from the European Research Council (ERC) under the European Union's Horizon 2020 research and innovation program, under grant agreement No. 648768; and from the *Agence Nationnale de la Recherche* (ANR) (No. ANR-14-CE14-0009-01) and from the Fondation pour la Recherche Médicale (FRM, No. ECO201906009090). This work was also supported by institutional grants from INSERM, CNRS, Aix-Marseille University and Marseille-Immunopole to the CIML.

Author contributions

G. H., G. D., A. Ro., R. R., P. V. B., A. B., designed and performed experiments and analyzed data. J.G. did the t-SNE analysis. C. L. and L.C. performed histological analysis. A.M. and A. Re. provided the GINIP-DTR and TAFA4-KO mice, reagents as well as important guidance for the characterization of sensory neurons. S. U. and G. H. designed the study, supervised experiments and co-wrote the manuscript. All authors reviewed and provided input on the manuscript.

Competing interests

S.U., G.H, G.D. and A.M. through Inserm transfert have filed a provisional international patent application WO2020/064907 on the clinical use of TAFA4. All other authors declare no competing interests.

Data availability

All data supporting the findings of this study are found within the manuscript and its Supplementary Information. Source data are provided with this paper.

Extended data legends

Extended data figure 1: UV overexposure triggers a sequence of skin inflammation and repair over 35 days and GINIP^{+} neurons activation

a, Heatmap representing the expression kinetics of genes involved in skin inflammation and repair over time (days) pi. Ears from WT mice were collected before UV irradiation (D0) or at D3, D7, D14 and D35 pi and total extracted RNA were analyzed by Fluidigm. Genes encoding proinflammatory cytokines and chemokines were expressed at D3 and D7 delineating the inflammatory phase (red cluster). Pro-repair genes were up-regulated at D14 and D35 (green cluster) delineating the resolution/remodeling phases. The gene *Fam19a4* encoding TAFA4 is highlighted in yellow (n=4-8 mice per group). **b,** Sensory neurons from C2/C3 DRGs innervate the ear skin**.** The fluorescent tracer DiI was injected intradermally in the right ears of WT mice and left ears were injected with PBS (n=3 independent DRGs per group). **c**, The trigeminal ganglia (TG) and cervical DRG (C2 to C5) were collected 48h post-injection and analyzed by fluorescent microscopy. **d**, Quantification of DiI^{+} neurons per DRG fields of view; PBS-injected control side (blue) or DiI-injected side (red). **e**, Additional representative confocal

961 images (related to main **figure 1c**) of C2 DRGs labeled for GINIP (red), CGRP (blue)
962 and ATF3 (green), from unexposed (left) and UV-exposed mice at D3 pi (right). **f**,
963 Quantification of total $GINIP^+$ and $CGRP^+$ neurons per DRGs (left) and total
964 $CGRP^+ATF3^+$ and $GINIP^+ATF3^+$ (right) from unexposed (blue) and UV-exposed mice
965 at D3 pi (red), (n=8 mice per group). All data are representative for at least two
966 independent experiments and presented as means ± SEM. One-way ANOVA with
967 Tukey's multiple comparisons test (ns: non-significant; *$p < 0.05$; **$p < 0.01$; ***$p <$
968 0.001).
969
970
971

Extended data figure 2: Conditional ablation of GINIP$^+$ neurons in GINIP-DTR mice and skin histopathological analysis after UV exposure.

a, Representative confocal images for DAPI (blue) and GINIP (green) staining of C3 DRGs from control DTR-control (upper panels) and GINIP-DTR (lower panels) mice, 10 weeks post-DT treatment. **b**, Absolute number of GINIP$^+$, CGRP$^+$, TAFA4$^+$, TH$^+$ and IB4$^+$ DRG neurons were quantified in DTR-control (blue) and GINIP-DTR mice (red), (n=4-6 independent DRG per group). **c**, Representative confocal images for Beta3-tubulin (blue) and GINIP (green) staining, of mouse ear skin sections as in **a**. **d**, scratching episodes were monitored during 30 min at each time point pi indicated (n=6-10 mice per group). **e**, Representative H&E staining of ears from DTR (left) and GINIP-DTR (right) mice at D35 pi. Histopathological analysis for leukocyte infiltration (**f**), epidermal thickness (**g**), fibrosis (**h**) and fibrosis extension (**i**) (n=5 mice per group) related to the main **Fig. 1g-j**. Criteria used for the histopathological scoring are described in the **Article Methods**. **j**, Representative Masson trichrome (upper panel) and H&E staining (lower panel) of back skin from DTR-control (left) and GINIP-DTR (right) mice at D35 pi. All data are representative for at least two independent experiments and presented as mean ± SEM. One-way ANOVA with Tukey's multiple comparisons test (ns: non-significant; *$p < 0.05$; **$p < 0.01$; ***$p < 0.001$).

Extended data figure 3: Immune cell subsets in the skin before and after UV exposure.

a, Flow cytometry gating strategy using CD11b, CD11c, CD64, MHC-II, CD103, c-kit, Ly6G and CD24 marker expression. Dendritic cells (DC; $CD11c^{+}MHCII^{+}$), mast cells (MC; $CD11b^{-}c\text{-}kit^{+}$), lymphoid cells (Lymϕ; $CD11b^{-}CD103^{-/+}$), granulocytes ($CD11b^{+}CD24^{+}$, $Ly6G^{+}$) and the monocyte/macrophage compartment (Mo/Mϕ; $CD11c^{-}MHCII^{-}CD11b^{+}CD24^{-}Ly6G^{-}CD64^{int/+}$) are shown. **b**, Absolute numbers per mg of skin for DC, MC, Lymϕ, Gr and Mo/Mϕ populations at D14 pi in DTR-control (blue) or GINIP-DTR (red) mice, (n=8 mice per group). **c**, Gating strategy for skin dendritic cell subsets ($CD11c^{+}MHCII^{+}$) and monitoring of Langerhans cells (LC; $EpCAM^{+}Langerin^{+}$), (n=5-8 mice per group). **d**, FACS plot for LC (left) and quantification (right) in DTR-control and GINIP-DTR mice, unexposed (No UV) or at D14 pi (UV), (n=5-10 mice per group). **e**, Percentage of LC among DC over time post-UV exposure in WT and Tafa4 KO mice. **f**, Representative flow cytometry analysis of skin immune cells and DRG neurons for the expression of DTR in GINIP-DTR mice. **g**, Confocal analysis of whole mount ear skin from Nav1.8-RFP mice stained for $GINIP^{+}$ neurons and $CD206^{+}$ dermal resident Mϕ. Hair follicles (HF) are highlighted within white dashed squares. In the skin, Nav1.8 expression (RFP) is restricted to sensory neuron axonal extensions. In DRG (**f**), DTR expression is restricted to neuronal cellular bodies in DRGs. These markers were not detected in immune cells. All data are representative for at least two independent experiments and presented as mean ± SEM. One-way ANOVA with Tukey's multiple comparisons test (ns: non-significant; $*p < 0.05$; $**p < 0.01$; $***p < 0.001$).

Extended data figure 4: Flow cytometry and t-SNE analysis of skin Monocyte/Macrophage subsets in GINIP-DTR mice.

a, Classical flow cytometry gating strategy for Monocyte and Macrophage (Mo/Mϕ) subsets in the skin. **b**, t-SNE analysis including CCR2, Ly6C, MHC-II, CD64, CD206 and Tim4 markers was performed to cluster Mo/Mϕ populations at day 14 pi in the skin of GINIP-DTR and DTR-control mice (See also **Article methods** for t-SNE analysis). **c**, Representative plots for $CCR2^{-/+}CD206^{-}$ monocyte subsets on D3, D7 and D14 pi in the skin of control (DTR) or GINIP-DTR mice. **d**, Absolute numbers of $Ly6C^{+}$ Mo, Int. Mo, PMo and MoDC subsets, per mg of ear skin (n=9-13 mice per group) as in **c**. **e**, Representative FACS plots for $CD206^{+}$ dermal resident Mϕ as in **c**. **f**, Absolute numbers of DN and MHC II^{+} Mϕ subsets, per mg of ear skin (n=9-13 mice per group) as in **c**. **g,** Representative FACS plots for $CD206^{+}$ dermal resident Mϕ subsets at D14 pi in back skin from control (DTR) or GINIP-DTR mice. **h**, Absolute numbers of Mϕ subsets, per mg of back skin (n=12 mice per group) from DTR-control (gray) or GINIP-DTR (colored) mice, at D14 pi. All data are representative for at least two independent experiments and presented as mean ± SEM. One-way ANOVA with Tukey's multiple comparisons test (ns: non-significant; $*p < 0.05$; $**p < 0.01$; $***p < 0.001$).

Extended data figure 5: GINIP$^+$ sensory neurons innervate hair follicles and release TAFA4 in the skin.

a, Representative confocal images of whole mount ear skin from WT mice stained with an anti-Beta3-tubulin (blue) and anti-GINIP (green) antibodies. GINIP$^+$ lanceolate barrel structures innervating hair follicles (HF) are highlighted within dashed squares. **b**, Confocal analysis as in **a** with an additional anti-TH antibody staining (red) shows GINIP$^+$TH$^+$ C-LTMR axon terminals reaching hair follicle. **c**, Schematically, GINIP$^+$ neurons consist of two subsets of sensory neurons projecting in the inter-follicular regions of the epidermis as free nerve endings (IB4$^+$) and hair follicles as C-LTMRs (TAFA4$^+$). **d**, Confocal images of DRG sections from control WT (left) or *Tafa4*-KO (right) mice after immunofluorescent (IF) staining with an anti-GINIP (green) an anti-TAFA4 antibody (1D8; red) and DAPI (blue). **e**, Additional confocal images of C3 DRGs (IF) stained with the isolectin B4 (blue), anti-TAFA4 (1D8, red), and ATF3 (green) antibodies, in WT mice (related to **main Figure 3**), unexposed (left) or at D3 pi (right). **f**, Absolute number of TAFA4$^+$ and IB4$^+$ neurons (left; n=6-12 mice per group) and absolute number of TAFA4$^+$ATF3$^+$ and IB4$^+$ATF3$^+$ neurons per DRG (right) from unexposed (blue) and exposed D3 pi (red) WT mice, (n=8 mice per group). **g**, DAPI staining (blue) *in situ* hybridization (ISH) for *Tafa4* mRNA (red) in DRG as in **d**. **h**, Quantification of TAFA4 levels (ELISA) in DRGs from WT mice unexposed (D0) to D14 pi. **i**, *Tafa4* mRNA expression (RT-qPCR) in peripheral tissues and DRGs (n=3 mice per time point; n.d: not determined). **j**, Quantification of *Tafa4* mRNA expression in PBMC, BM, BMDM and sorted CD206$^+$ dermal Mϕ compared to DRGs (n=3 independent samples). **k**, *Tafa4* mRNA expression in C3 DRGs from D0 to D35 pi (n=3 mice per time point). All data are representative for at least two independent experiments and presented as mean ± SEM. One-way ANOVA with Tukey's multiple

comparisons test except **h**, Kruskal-Wallis (ns: non-significant; *$p < 0.05$; **$p < 0.01$; ***$p < 0.001$).

Extended data figure 6: Tafa4 regulates skin inflammation after UV exposure but does not affect Treg and Mast cell IL-10 production.

a, Changes in ear skin thickness over time pi in WT control (blue) and *Tafa4*-KO (red) mice (*n*=9 mice per group). **b**, Representative H&E images of ears from WT (left) or *Tafa4*-KO (right) mice at D35 pi and histopathological scoring for leukocyte infiltration, epidermal thickness, fibrosis, fibrosis extension and then **c**, cumulative fibrosis score and total pathological scores (n=12 mice per group). See detailed scoring in **Article methods**. **d,** IL-6, IL-1β, and chemokines CCL2, CXCL1 and CCL4 protein levels (measured by CBA) and *Il10* mRNA level, in ear skin from WT (blue) or *Tafa4*-KO (red) mice from D0 to D35 pi (n=3-11 mice per group and time point). **e**, FACS analysis and detection of IL-10^{+} immune cells from control (WT; gray) and IL-10-GFP (red) mice using an anti-GFP antibody and **f**, using an anti-IL-10 antibody, in skin DC subsets, Lymϕ cells, monocytes, mast cells (MC) and Mϕ subsets in control (IL-$10^{gfp/gfp}$ mice, gray) and WT (blue) mice. **g**, Gating strategy for Tregs ($CD4^{+}TCR\beta^{+}FoxP3^{+}$) and **h**, absolute number per mg of ear skin before (D0) or pi, in DTR-control (blue) or GINIP-DTR (red) mice (n=9-18 mice per group and per time point). **i**, Representative FACS plots for IL-10 in Tregs from WT (left) or *Tafa4*-KO (right) mice before (blue) or pi (red). **j**, Gating strategy (left) and absolute number (right) of mast cells (MC) per mg of skin from DTR-control (blue) or GINIP-DTR (red) mice, showing MC depletion (D3) and repopulation (D7) after UV exposure; (n=8-9 mice per group and time point). **k**, Representative FACS plots for IL-10 in $Tim4^{+}$ Mϕ (blue) and MC (yellow) before (No UV, top) and at D10 pi (bottom) in WT mice. **l**, Representative FACS plot for IL-10 in MC in WT (blue) or *Tafa4*-KO (red) mice at D10 pi and **m**, median IL-10 MFI analysis (n=6-10 mice per group). All data are representative for at least two independent experiments and presented as mean ± SEM. One-way ANOVA with

Tukey's multiple comparisons test (ns: non-significant; *$p < 0.05$; **$p < 0.01$; ***$p < 0.001$).

Extended data figure 7: TAFA4 promotes IL-10 production by dermal resident Mϕ subsets *in vivo* and directly up-regulates *Il10* in Mϕ *in vitro*.

Representative FACS plots (upper panels) for intracellular IL-10 expression in DN Mϕ (**a**), MHC-II$^+$ Mϕ (**b**) and Tim4$^+$ Mϕ (**c**) subsets from WT (blue) and *Tafa4*-KO (red) mice at D10 pi, and (lower panels) median IL-10 MFI quantifications in the respective Mϕ subsets at D3, 7 and 10 pi (n=6-9 mice per group and time point). **d**, BMDM, derived from WT or FPR1-KO bone marrow, were challenged in a migration assay (transwell) using medium alone (CTL$^-$), MCP-1 (CTL$^+$) or increasing concentrations of TAFA4. Absolute number of Mϕ in the bottom wells were analyzed by FACS (n=3 independent samples per group). **e**, *IL6* mRNA level in ThioMϕ in the presence (green) or absence (blue) of TAFA4 (See main **Fig.4i**), (n=6-8 independent sample per group). **f**, BMDM as in (**d**), were activated in vitro by LPS alone (blue) or in the presence of TAFA4 (green). Gene expression was analyzed by RT-qPCR for *Tnfa*, *Il6* and *Il10* and compared to non-activated BMDM (CTL), (n=4-5 independent sample). All data are representative for at least two independent experiments and presented as mean ± SEM. One-way ANOVA with Tukey's multiple comparisons test (*$p < 0.05$; **$p < 0.01$; ***$p < 0.001$).

Extended data figure 8: Fate-mapping and shield irradiated BM chimeras revealed that TAFA4 regulates the dynamic between embryo-derived- and monocyte-derived Mϕ after UV exposure.

a, Strategy for embryonic progenitor fate mapping using the CX3CR1$^{CreERT2:R26\text{-}YFP}$ mice. Tamoxifen (Tam) was injected in pregnant females at E16.5 days of pregnancy and offsprings were analyzed at 6 weeks of age. **b**, Percentages of YFP$^+$ cells in the indicated cell types (n=5 mice). LCs: Langerhans cells. **c**, Experimental scheme for monocyte tracing using CD45.1$^+$ BM shield-irradiated chimeras. **d**, Percentage of CD45.1 chimerism within the indicated Mo/Mϕ subsets in 2 months old chimeric mice in the steady state (n=7 mice per group), or **e**, after additional 4 months following UV irradiation (purple) or no UV (gray), (n=5 mice per group). **f**, Gating strategy for Mo/Mϕ analysis in WT CD45.1 BM Chimera before UV exposure (top panels) and then at D7 pi in WT (middle panels) and in *Tafa4*-KO (bottom panels) recipient chimeras. **g**, Relative expression of the markers CD45.1, Ly6C, CD64, CD206, MHCII and Tim4 used for t-SNE analysis of skin Mo/Mϕ subsets from WT or Tafa4-KO recipient chimeras (see also **Fig. 4a**). **h**, Absolute numbers (n=9 mice per group) per mg of ear skin (left) and CD45.1 chimerism levels (right) (n=7 mice per group) for DN Mϕ and MHC-II$^+$ Mϕ in WT (blue) and *Tafa4*-KO (red) BM-chimeric mice on D7 pi. **i**, Representative Annexin-V staining of DN Mϕ (left), MHC-II$^+$ Mϕ (middle) and Tim4$^+$ Mϕ (right) at D3 pi from DTR (blue) or GINIP-DTR (red) mice. **j**, median MFI for annexin-V in Mϕ subsets as in (**i**), (n=4 mice per group). **k**, Representative Annexin-V as in (**i**) at D2 pi for WT (blue) or *Tafa4*-KO (red) mice. **l**, Median fluorescence intensity (MFI) for Annexin-V in Mϕ subsets as in (**j**), (n=5-6 mice per group). All data are representative for at least two independent experiments and presented as mean ±

SEM. One-way ANOVA with Tukey's multiple comparisons test (ns: non-significant; *$p < 0.05$; **$p < 0.01$; ***$p < 0.001$).

Extended data figure 9: IL-10 defect and dermal Mϕ depletion recapitulate *Tafa4*-KO mice phenotype after UV exposure.

a, Experimental scheme for *in vivo* neutralization of IL-10 in WT mice. **b**, Ear thickness at D14 pi, of WT (blue) or *Tafa4*-KO (red) mice treated with an IgG2a isotype control (iso) and of WT mice treated with anti-IL-10 blocking antibodies (purple), (n=10 mice per group). **c**, Absolute numbers of Inflam Mϕ (left) and $Tim4^+$ Mϕ (right) in ear skin of the indicated 3 groups of mice (as in **b**), (n=6-9 mice per group). **d**, Representative FACS plots of Mo/Mϕ subsets at D0 and D3 pi in IL-$10^{wt/gfp}$ and IL-$10^{gfp/gfp}$ (IL-10 KO) mice. **e**, Absolute number of $Tim4^+$ Mϕ (left) and Inflam Mϕ (right) per mg of skin at D7 pi in IL-$10^{wt/gfp}$ (gray) and IL-$10^{gfp/gfp}$ (colored), (n=8-10 mice per group). **f**, ear thickness before (No UV) and at D14 pi (UV) in IL-$10^{wt/gfp}$ (blue) and IL-$10^{gfp/gfp}$ (purple) mice, (n=9-12 mice per group). **g**, Experimental scheme for dermal resident Mϕ depletion: two i.p. injections, at D-3 and D-2, of the CSF-1R blocking antibody AFS98, are effective to deplete DN, $Tim4^+$, MHC II^+ and Langerhans cells in WT mice. **h**, Absolute number of Mϕ per mg of ear skin before (CTL) and after AFS98 injection (colored), (n= 13 mice per group). **i**, IL-10 protein level detected by CBA in WT (blue) and *Tafa4*-KO (red) after isotype control or AFS98 antibody injection (n=4-5 mice per group). **j**, Absolute number of myeloid cell subsets per mg of ear skin after isotype control or AFS98 antibody injection (colored), (n= 11 mice per group). **k**, (left) Representative FACS plots of Mo/Mϕ subsets over the time course of Mϕ repopulation (D0, D2, and D4) after AFS98 injection and complete Mϕ depletion (D0) in WT mice, and, (right) Representative FACS plots at D6 after AFS98 injection in WT (blue) and *Tafa4*-KO (red) mice showing the acquisition of Tim4 by monocytes-derived Mϕ, (see bottom panels). **l**, Representative FACS plots of Mo/Mϕ subsets at D0 and D3 post-UV exposure in WT and *Tafa4*-KO mice after Mϕ depletion with the blocking anti-CSF-

1R Ab (AFS98). Absolute number of Tim4^{+} Mϕ **m** (left), and Inflam Mϕ (right**)**, per mg of skin at D7 pi in WT (gray) and *Tafa4*-KO (colored) treated with an IgG2a isotype control (Iso+UV), or treated with anti-CSF-1R Ab (AFS+UV), (n=8-9 mice per group). **n**, ear thickness in unexposed mice (No UV), and at D14 pi in WT (blue) and *Tafa4*-KO (red) mice treated as in **m** (n=10 mice per group). All data are representative for at least two independent experiments and presented as mean ± SEM. One-way ANOVA with Tukey's multiple comparisons test (ns: non-significant; *$p < 0.05$; **$p < 0.01$; ***$p < 0.001$).

Extended data figure 10: Adoptive transfer of Tim4$^+$ macrophages is sufficient to reduce tissue damage in GINIP-DTR mice.

a, Experimental scheme for intradermal adoptive transfer of CD45.1$^+$Tim4$^+$ Mϕ**. b,** Gating strategy for sorting CD45.1$^+$ Inflam Mϕ (pink) and Tim4$^+$ Mϕ (cyan). **c**, ear thickness for unexposed (No UV) or UV-exposed mice at D7 pi, in DTR (blue), GINIP-DTR (red) mice and GINIP-DTR mice injected with Inflam Mϕ (pink) or with Tim4$^+$ Mϕ (cyan) mice, (n=7-10 mice per group). **d**, Representative images of ears at D7 pi from each group as in (**c**). **e**, Experimental scheme for TAFA4 rescue in *Tafa4*-KO mice. **f**, Representative FACS plot for intracellular staining of IL-10 in Tim4$^+$ Mϕ at D14 pi, in WT mice treated with saline (blue) or *Tafa4*-KO mice treated with saline (red) or *Tafa4*-KO mice treated with TAFA4 (green). **g**, Model for TAFA4 functions *in vivo* after UV exposure: 1) Role of TAFA4 during the inflammatory phase. Skin overexposure to UV induces the release of the neuropeptide TAFA4 by C-LTMRs. TAFA4 promotes the production of IL-10 by embryonic-derived dermal resident Tim4$^+$ Mϕ. The production of IL-10 is essential for their survival and protect the skin from over-inflammation. Tissue lesions also induce the recruitment of monocytes in the skin, where they differentiate into TNFα$^+$ Inflam Mϕ. In the absence of TAFA4 production, the number of Tim4$^+$ Mϕ and IL-10 levels are reduced, promoting the expansion of Inflam Mϕ. 2) Role of TAFA4 during the resolution phase. The TAFA4/IL-10 axis is still active, promoting the maintenance of both embryonic- and monocyte-derived IL-10$^+$ Tim4$^+$ Mϕ, which are required for tissue repair. In the absence of TAFA4 production, IL-10 production by the three subsets of CD206$^+$ dermal Mϕ is compromised, leading to persistent inflammation and fibrotic scars. **h**, Repeated measure over time of ear thickness changes (μm) of WT (blue) and *Tafa4*-KO (red) mice treated daily with Imiquimod (IMQ) during six consecutive days and followed up

to 15 days, (n=5 mice per group). All data are representative for at least two independent experiments and presented as mean ± SEM. One-way ANOVA with Tukey's multiple comparisons test (ns: non-significant; *$p < 0.05$; **$p < 0.01$; ***$p < 0.001$).

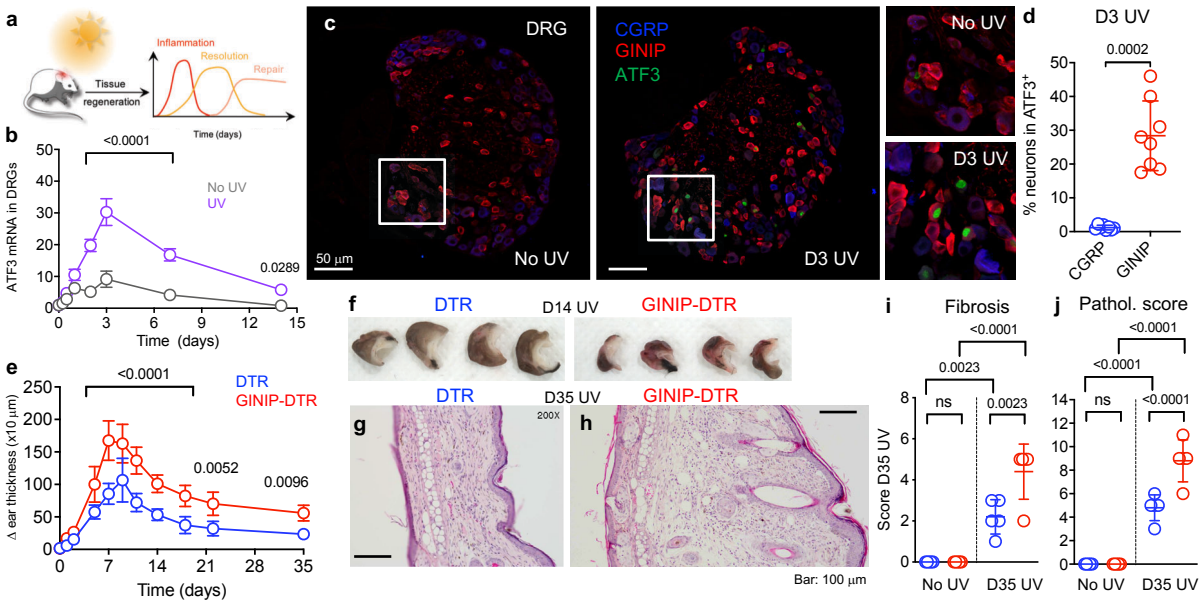
a
Inflammation
Resolution
Repair
Tissue regeneration
Time (days)
b
ATF3 mRNA in DRGs
<0.0001
No UV
UV
0.0289
Time (days)
c
DRG
50 µm
No UV
CGRP
GINIP
ATF3
D3 UV
No UV
D3 UV
d
D3 UV
0.0002
% neurons in ATF3+
CGRP
GINIP
e
Δ ear thickness (x10 µm)
<0.0001
DTR
GINIP-DTR
0.0052
0.0096
Time (days)
f
DTR
D14 UV
GINIP-DTR
DTR
D35 UV
GINIP-DTR
g
200X
h
Bar: 100 µm
i
Fibrosis
<0.0001
0.0023
ns
0.0023
Score D35 UV
No UV
D35 UV
j
Pathol. score
<0.0001
<0.0001
ns
<0.0001
No UV
D35 UV

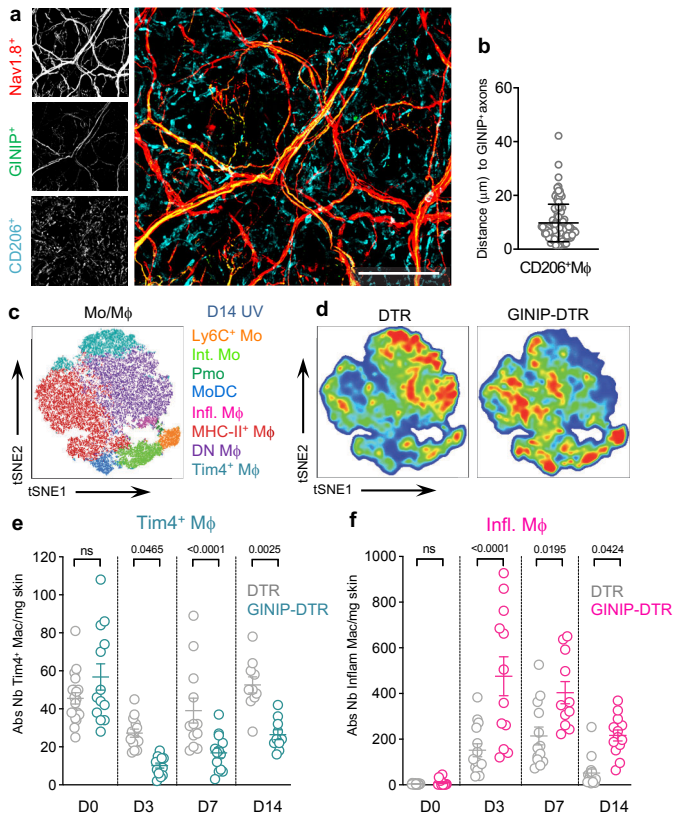
a
Nav1.8+
GINIP+
CD206+
b
Distance (µm) to GINIP+ axons
60
40
20
0
CD206+Mϕ
c
Mo/Mϕ
D14 UV
Ly6C+ Mo
Int. Mo
Pmo
MoDC
Infl. Mϕ
MHC-II+ Mϕ
DN Mϕ
Tim4+ Mϕ
tSNE2
tSNE1
d
DTR
GINIP-DTR
tSNE2
tSNE1
e
Tim4+ Mϕ
Abs Nb Tim4+ Mac/mg skin
ns
0.0465
<0.0001
0.0025
DTR
GINIP-DTR
120
100
80
60
40
20
0
D0
D3
D7
D14
f
Infl. Mϕ
Abs Nb Inflam Mac/mg skin
ns
<0.0001
0.0195
0.0424
DTR
GINIP-DTR
1000
800
600
400
200
0
D0
D3
D7
D14

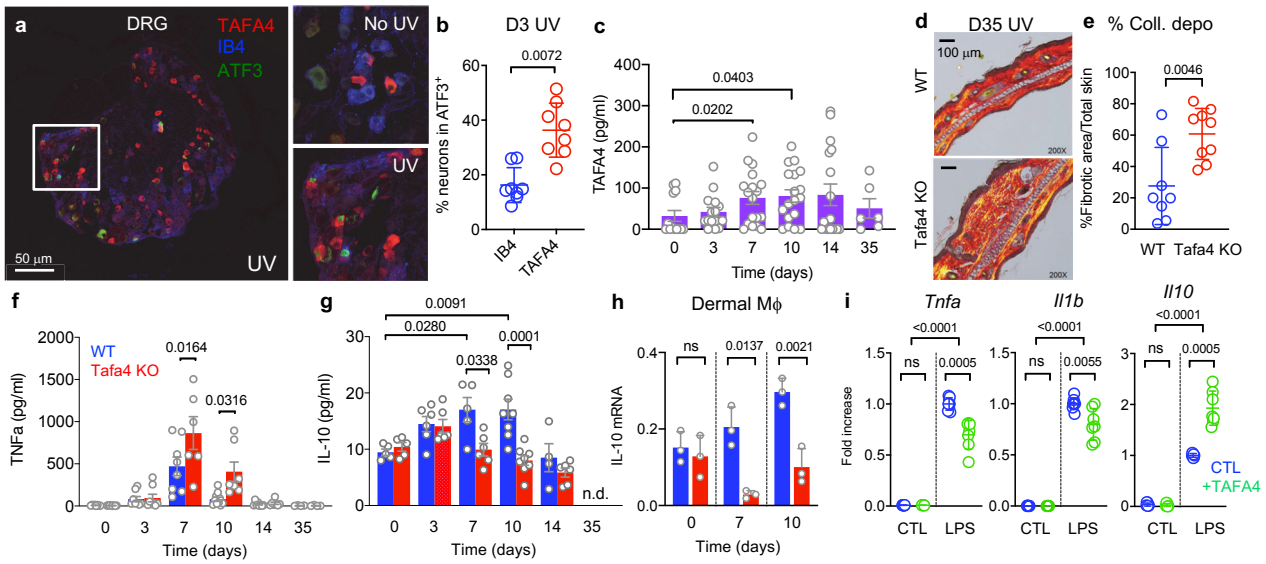
a
DRG
TAFA4
IB4
ATF3
50 µm
UV
No UV
UV
b
D3 UV
0.0072
% neurons in ATF3+
IB4
TAFA4
c
0.0403
0.0202
TAFA4 (pg/ml)
Time (days)
d
D35 UV
100 µm
WT
Tafa4 KO
200X
e
% Coll. depo
0.0046
%Fibrotic area/Total skin
WT
Tafa4 KO
f
WT
Tafa4 KO
0.0164
0.0316
TNFa (pg/ml)
Time (days)
g
0.0091
0.0280
0.0338
0.0001
IL-10 (pg/ml)
n.d.
Time (days)
h
Dermal Mϕ
ns
0.0137
0.0021
IL-10 mRNA
Time (days)
i
Tnfa
Il1b
Il10
<0.0001
ns
0.0005
0.0055
Fold increase
CTL
LPS
CTL
+TAFA4

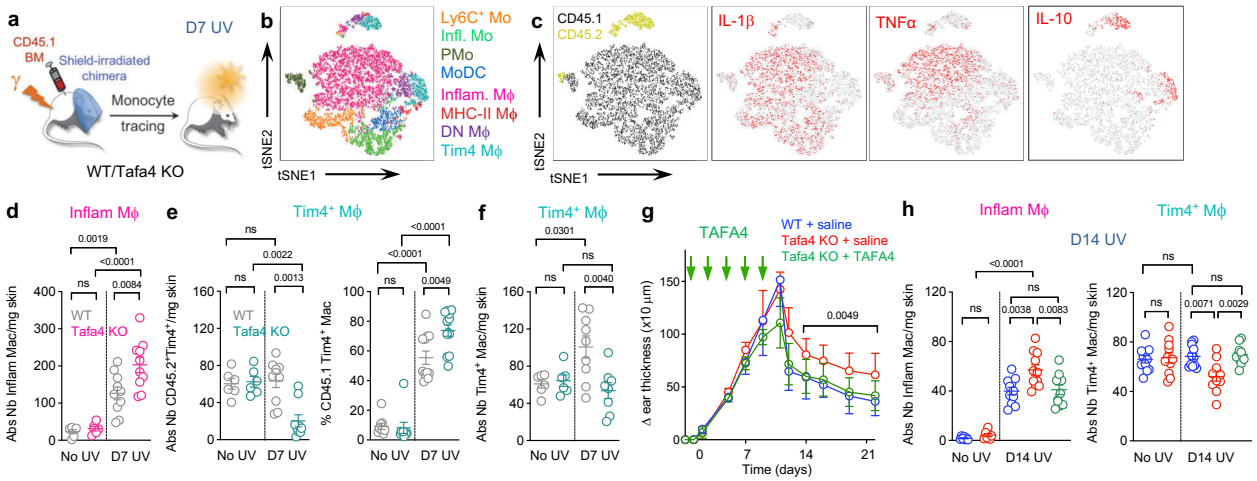
a
CD45.1
BM
Shield-irradiated chimera
γ
Monocyte tracing
D7 UV
WT/Tafa4 KO
b
tSNE2
tSNE1
Ly6C+ Mo
Infl. Mo
PMo
MoDC
Inflam. Mϕ
MHC-II Mϕ
DN Mϕ
Tim4 Mϕ
c
CD45.1
CD45.2
IL-1β
TNFα
IL-10
d
Inflam Mϕ
Abs Nb Inflam Mac/mg skin
WT
Tafa4 KO
No UV
D7 UV
e
Tim4+ Mϕ
Abs Nb CD45.2+Tim4+/mg skin
% CD45.1 Tim4+ Mac
f
Abs Nb Tim4+ Mac/mg skin
g
TAFA4
WT + saline
Tafa4 KO + saline
Tafa4 KO + TAFA4
Δ ear thickness (x10 µm)
Time (days)
h
D14 UV
D14 UV

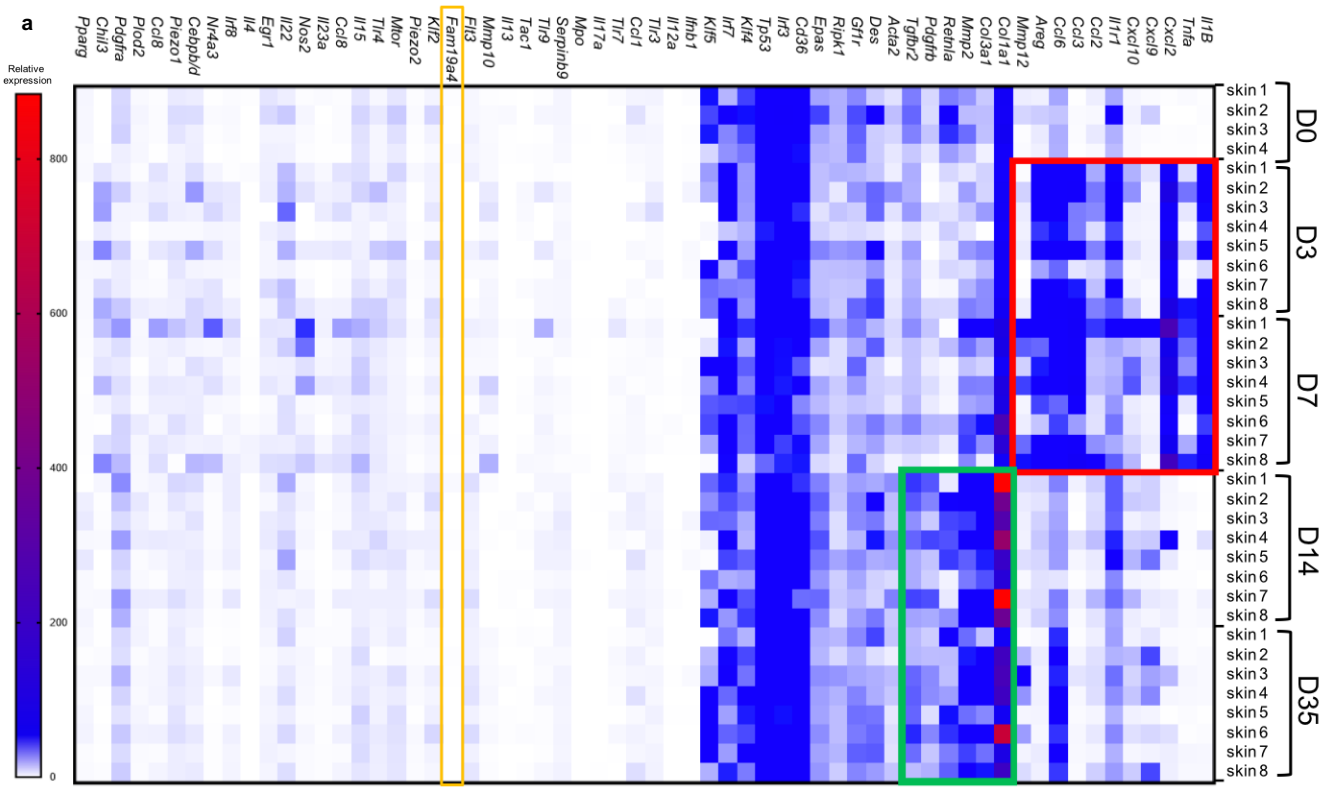

Identification of DRGs innervating the ear skin by DiI retrolabeling

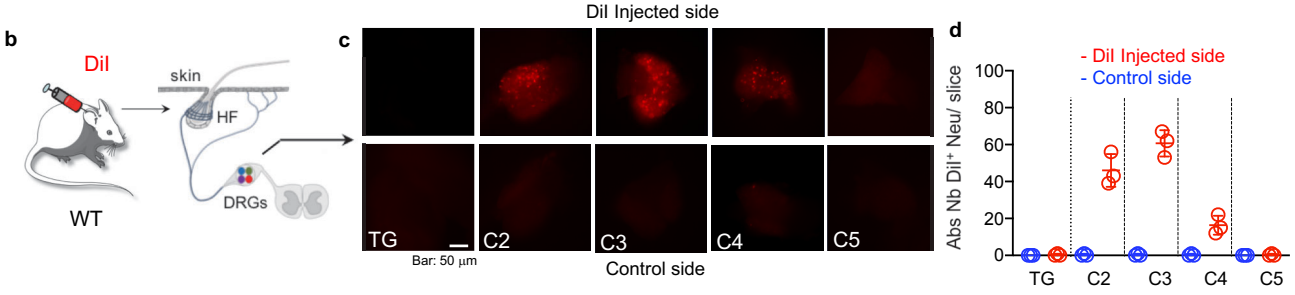

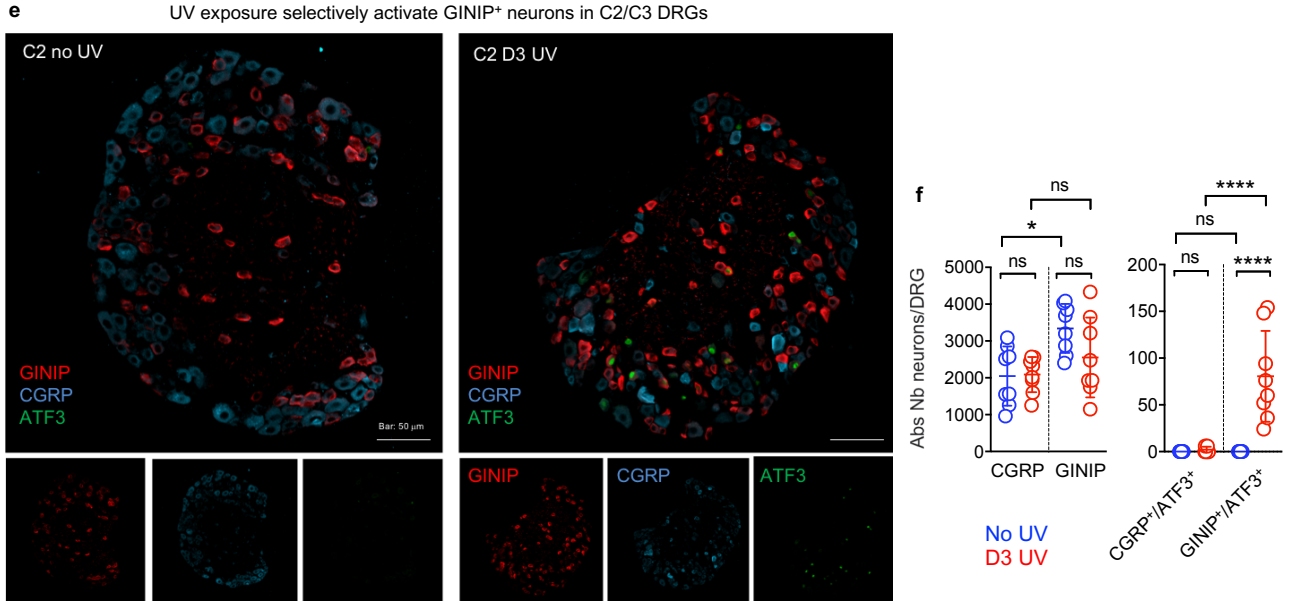

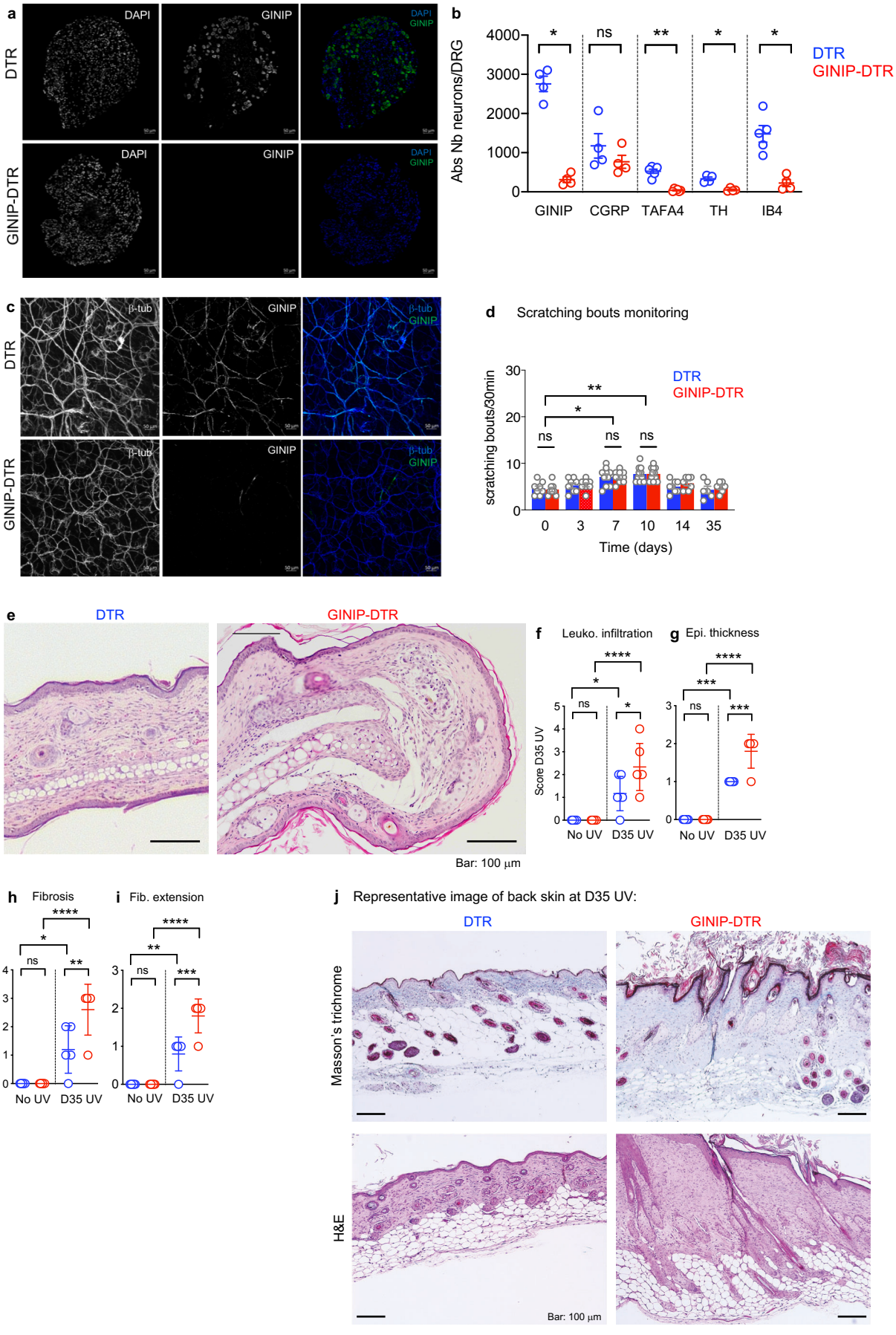
a
DTR
GINIP-DTR
DAPI
GINIP
DAPI
GINIP
b
Abs Nb neurons/DRG
4000
3000
2000
1000
0
*
ns
**
*
*
GINIP
CGRP
TAFA4
TH
IB4
DTR
GINIP-DTR
c
β-tub
GINIP
β-tub
GINIP
d
Scratching bouts monitoring
scratching bouts/30min
30
20
10
0
**
*
ns
ns
ns
0
3
7
10
14
35
Time (days)
DTR
GINIP-DTR
e
DTR
GINIP-DTR
Bar: 100 µm
f
Leuko. infiltration
Score D35 UV
****
*
ns
*
No UV
D35 UV
g
Epi. thickness
****
***
ns
***
No UV
D35 UV
h
Fibrosis
****
*
ns
**
No UV
D35 UV
i
Fib. extension
****
**
ns
***
No UV
D35 UV
j
Representative image of back skin at D35 UV:
DTR
GINIP-DTR
Masson's trichrome
H&E
Bar: 100 µm

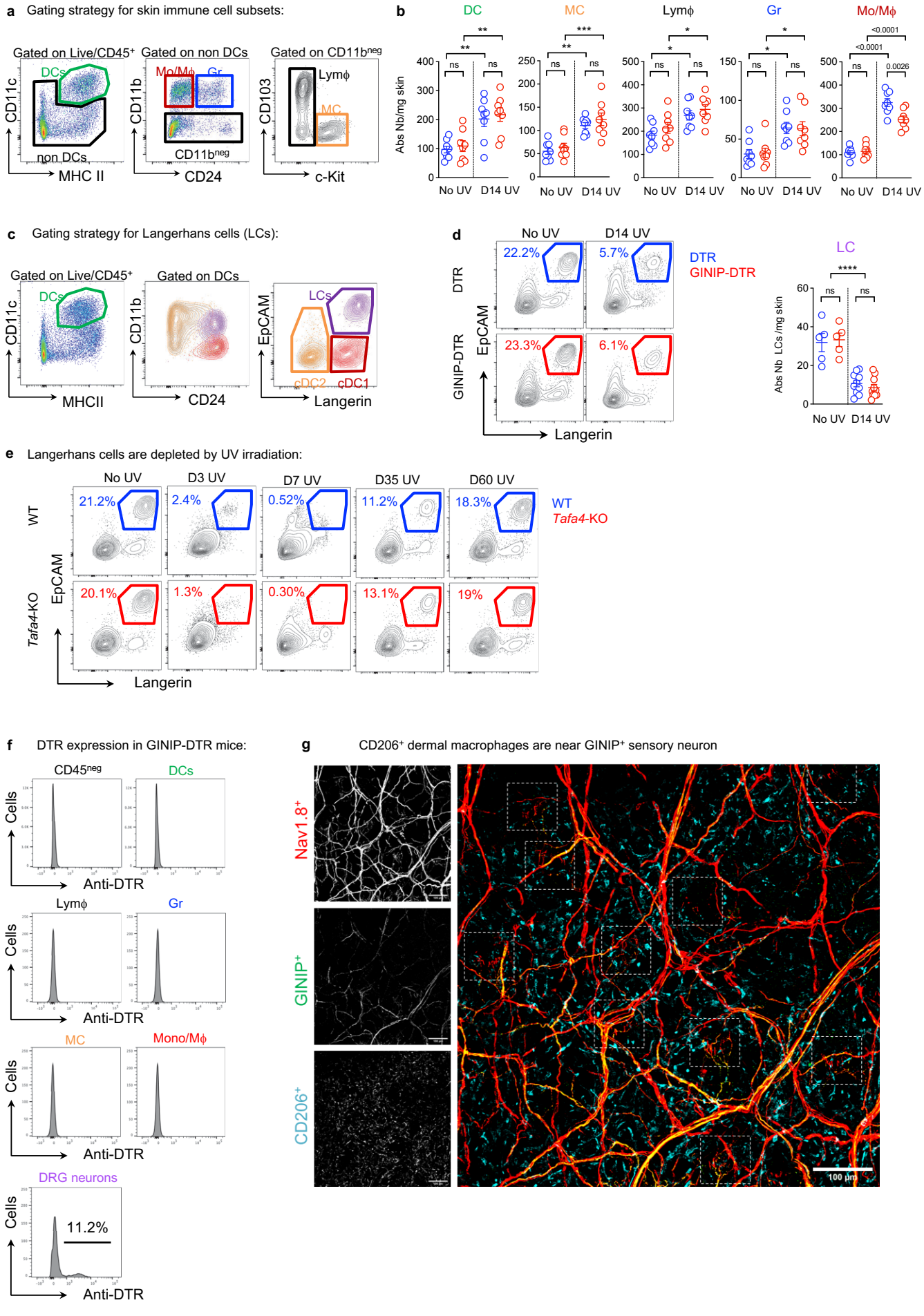
a Gating strategy for skin immune cell subsets:
Gated on Live/CD45+
Gated on non DCs
Gated on CD11bneg
DCs
non DCs
Mo/Mϕ
Gr
CD11bneg
Lymϕ
MC
CD11c
MHC II
CD11b
CD24
CD103
c-Kit
b
DC
MC
Lymϕ
Gr
Mo/Mϕ
Abs Nb/mg skin
ns
**
***
*
<0.0001
0.0026
No UV
D14 UV
c Gating strategy for Langerhans cells (LCs):
Gated on Live/CD45+
Gated on DCs
DCs
LCs
cDC2
cDC1
CD11c
MHCII
CD11b
CD24
EpCAM
Langerin
d
No UV
D14 UV
DTR
GINIP-DTR
22.2%
5.7%
23.3%
6.1%
EpCAM
Langerin
LC
****
Abs Nb LCs /mg skin
e Langerhans cells are depleted by UV irradiation:
No UV
D3 UV
D7 UV
D35 UV
D60 UV
WT
Tafa4-KO
21.2%
2.4%
0.52%
11.2%
18.3%
20.1%
1.3%
0.30%
13.1%
19%
EpCAM
Langerin
f DTR expression in GINIP-DTR mice:
CD45neg
DCs
Lymϕ
Gr
MC
Mono/Mϕ
DRG neurons
Cells
Anti-DTR
11.2%
g CD206+ dermal macrophages are near GINIP+ sensory neuron
Nav1.8+
GINIP+
CD206+
100 µm

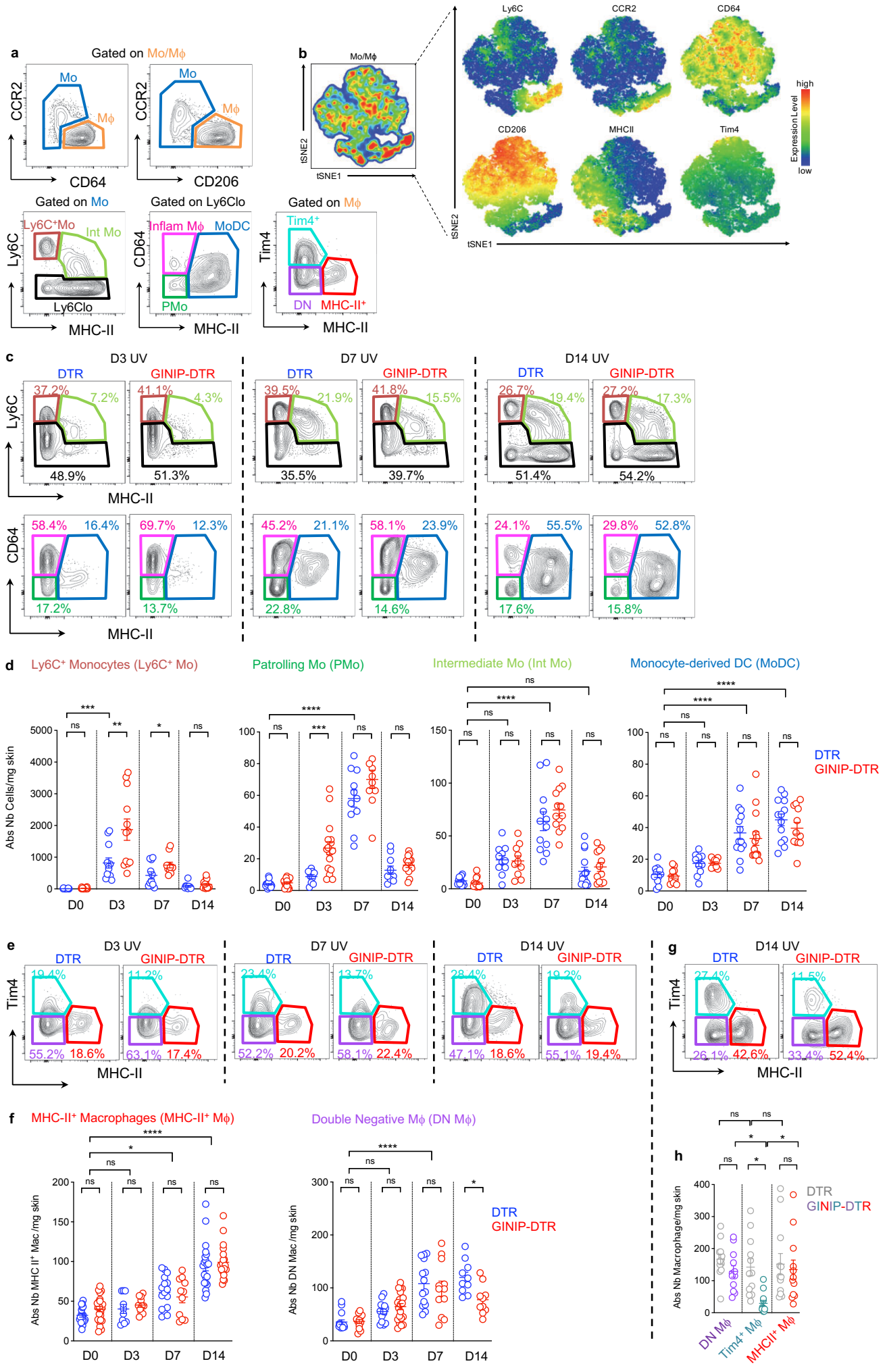
a
Gated on Mo/Mϕ
Mo
Mϕ
CCR2
CD64
CD206
Gated on Mo
Ly6C⁺Mo
Int Mo
Ly6Clo
Ly6C
MHC-II
Gated on Ly6Clo
Inflam Mϕ
MoDC
PMo
CD64
Gated on Mϕ
Tim4⁺
DN
MHC-II⁺
Tim4
b
Mo/Mϕ
tSNE1
tSNE2
Ly6C
CCR2
CD64
CD206
MHCII
Tim4
high
low
Expression Level
c
D3 UV
D7 UV
D14 UV
DTR
GINIP-DTR
37.2%
7.2%
48.9%
41.1%
4.3%
51.3%
39.5%
21.9%
35.5%
41.8%
15.5%
39.7%
26.7%
19.4%
51.4%
27.2%
17.3%
54.2%
58.4%
16.4%
17.2%
69.7%
12.3%
13.7%
45.2%
21.1%
22.8%
58.1%
23.9%
14.6%
24.1%
55.5%
17.6%
29.8%
52.8%
15.8%
d
Ly6C⁺ Monocytes (Ly6C⁺ Mo)
Patrolling Mo (PMo)
Intermediate Mo (Int Mo)
Monocyte-derived DC (MoDC)
Abs Nb Cells/mg skin
D0
D3
D7
D14
DTR
GINIP-DTR
e
D3 UV
D7 UV
D14 UV
DTR
GINIP-DTR
19.4%
55.2%
18.6%
11.2%
63.1%
17.4%
23.4%
52.2%
20.2%
13.7%
58.1%
22.4%
28.4%
47.1%
18.6%
19.2%
55.1%
19.4%
Tim4
MHC-II
g
D14 UV
DTR
GINIP-DTR
27.4%
26.1%
42.6%
11.5%
33.4%
52.4%
Tim4
MHC-II
f
MHC-II⁺ Macrophages (MHC-II⁺ Mϕ)
Double Negative Mϕ (DN Mϕ)
Abs Nb MHC II⁺ Mac /mg skin
Abs Nb DN Mac /mg skin
D0
D3
D7
D14
DTR
GINIP-DTR
h
Abs Nb Macrophage/mg skin
DN Mϕ
Tim4⁺ Mϕ
MHCII⁺ Mϕ
DTR
GINIP-DTR

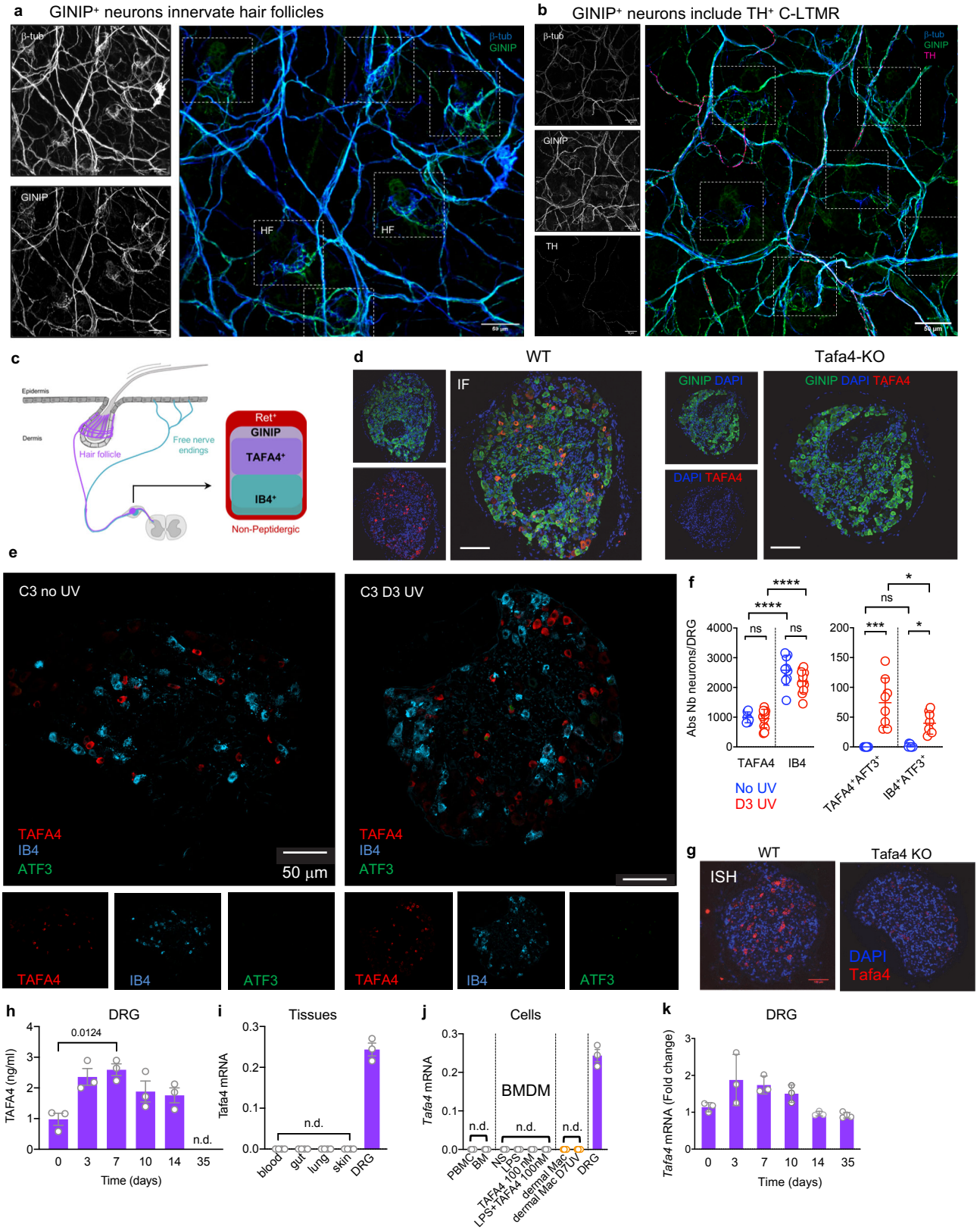
a
GINIP⁺ neurons innervate hair follicles
β-tub
GINIP
HF
HF
b
GINIP⁺ neurons include TH⁺ C-LTMR
β-tub
GINIP
TH
c
Epidermis
Dermis
Hair follicle
Free nerve endings
Ret⁺
GINIP
TAFA4⁺
IB4⁺
Non-Peptidergic
d
WT
Tafa4-KO
IF
GINIP DAPI
DAPI TAFA4
GINIP DAPI TAFA4
e
C3 no UV
C3 D3 UV
TAFA4
IB4
ATF3
50 µm
f
Abs Nb neurons/DRG
TAFA4
IB4
No UV
D3 UV
TAFA4⁺AFT3⁺
IB4⁺ATF3⁺
ns
****
***
*
g
WT
Tafa4 KO
ISH
DAPI
Tafa4
h
DRG
TAFA4 (ng/ml)
0.0124
n.d.
Time (days)
i
Tissues
Tafa4 mRNA
n.d.
blood
gut
lung
skin
DRG
j
Cells
Tafa4 mRNA
BMDM
n.d.
PBMC
BM
NS
LPS 100 nM
TAFA4 100nM
LPS+TAFA4 100nM
dermal Mac
dermal Mac D1UV
DRG
k
DRG
Tafa4 mRNA (Fold change)
Time (days)

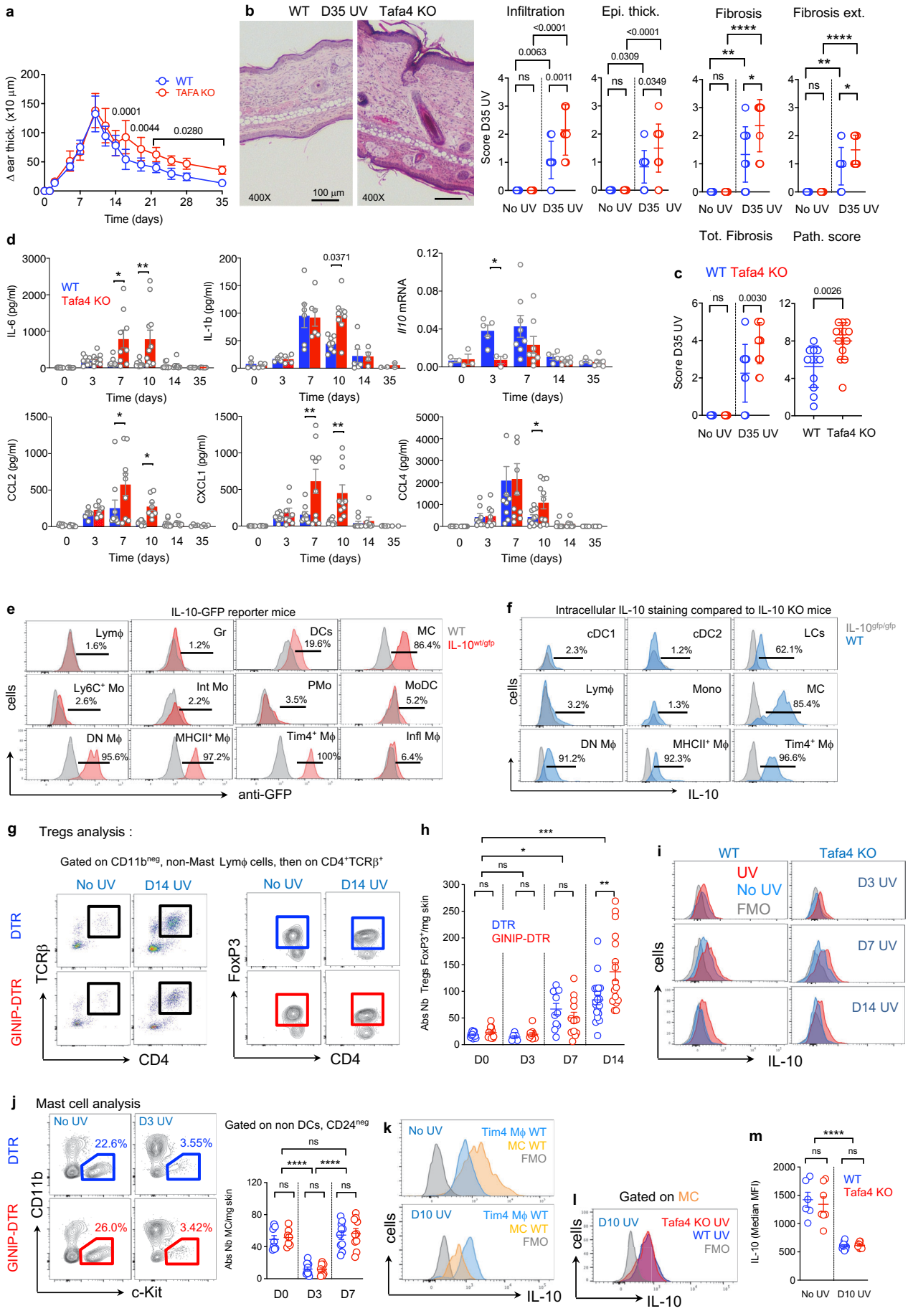
a
Δ ear thick. (x10 µm)
WT
TAFA KO
0.0001
0.0044
0.0280
Time (days)
b
WT D35 UV Tafa4 KO
400X
100 µm
Infiltration
Epi. thick.
Fibrosis
Fibrosis ext.
Score D35 UV
No UV D35 UV
Tot. Fibrosis
Path. score
c
WT Tafa4 KO
d
IL-6 (pg/ml)
IL-1b (pg/ml)
Il10 mRNA
CCL2 (pg/ml)
CXCL1 (pg/ml)
CCL4 (pg/ml)
e
IL-10-GFP reporter mice
Lymϕ
Gr
DCs
MC
Ly6C+ Mo
Int Mo
PMo
MoDC
DN Mϕ
MHCII+ Mϕ
Tim4+ Mϕ
Infl Mϕ
cells
anti-GFP
f
Intracellular IL-10 staining compared to IL-10 KO mice
cDC1
cDC2
LCs
Mono
IL-10
g
Tregs analysis :
Gated on CD11b^neg, non-Mast Lymϕ cells, then on CD4+TCRβ+
No UV
D14 UV
DTR
GINIP-DTR
TCRβ
FoxP3
CD4
h
DTR
GINIP-DTR
Abs Nb Tregs FoxP3+/mg skin
D0
D3
D7
D14
i
WT
Tafa4 KO
UV
No UV
FMO
D3 UV
D7 UV
D14 UV
j
Mast cell analysis
No UV
D3 UV
22.6%
3.55%
26.0%
3.42%
CD11b
c-Kit
Gated on non DCs, CD24^neg
Abs Nb MC/mg skin
k
No UV
Tim4 Mϕ WT
MC WT
FMO
D10 UV
l
Gated on MC
Tafa4 KO UV
WT UV
m
IL-10 (Median MFI)
WT
Tafa4 KO

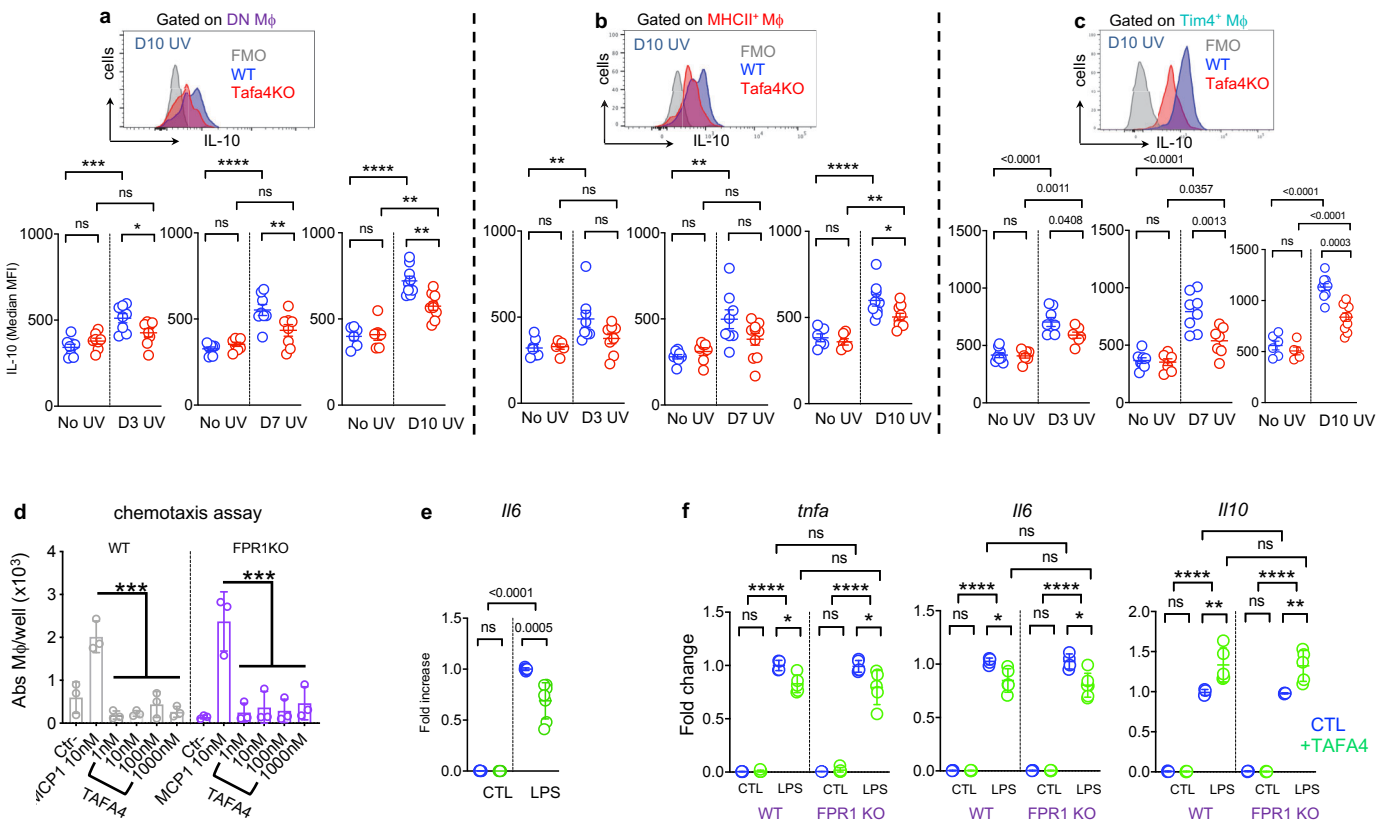
a
Gated on DN Mϕ
D10 UV
FMO
WT
Tafa4KO
cells
IL-10
IL-10 (Median MFI)
No UV
D3 UV
D7 UV
D10 UV
b
Gated on MHCII+ Mϕ
c
Gated on Tim4+ Mϕ

d
chemotaxis assay
WT
FPR1KO
Abs Mϕ/well (x10³)
Ctr-
MCP1 10nM
1nM
10nM
100nM
1000nM
TAFA4
e
Il6
Fold increase
CTL
LPS
f
tnfa
Il6
Il10
Fold change
WT
FPR1 KO
CTL
+TAFA4

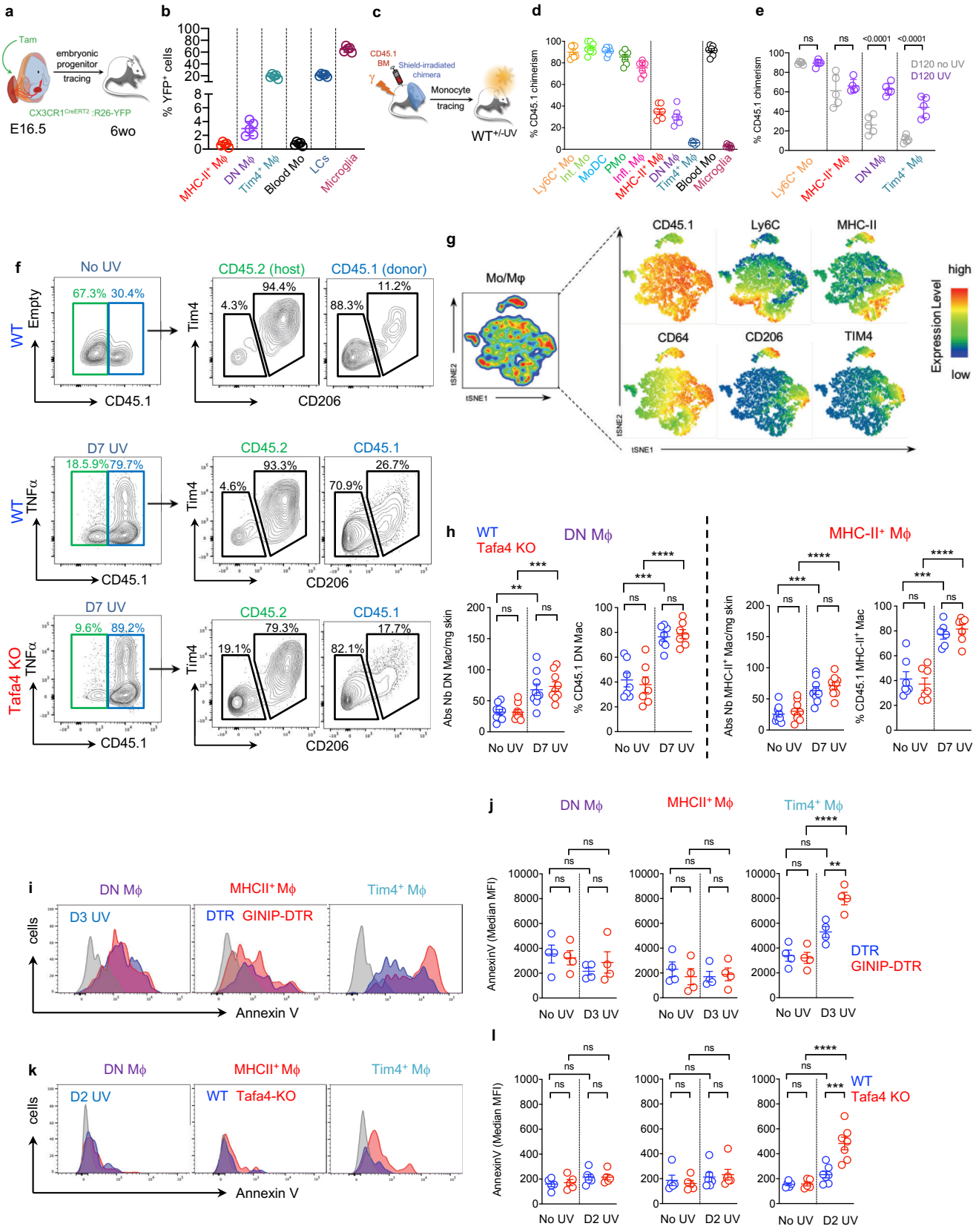
a
Tam
embryonic progenitor tracing
CX3CR1CreERT2 :R26-YFP
E16.5
6wo
b
% YFP+ cells
MHC-II+ Mϕ
DN Mϕ
Tim4+ Mϕ
Blood Mo
LCs
Microglia
c
CD45.1 BM
Shield-irradiated chimera
γ
Monocyte tracing
WT+/-UV
d
% CD45.1 chimerism
Ly6C+ Mo
Int. Mo
MoDC
PMo
Infl. Mϕ
MHC-II+ Mϕ
DN Mϕ
Tim4+ Mϕ
Blood Mo
Microglia
e
% CD45.1 chimerism
ns
<0.0001
D120 no UV
D120 UV
Ly6C+ Mo
MHC-II+ Mϕ
DN Mϕ
Tim4+ Mϕ
f
No UV
CD45.2 (host)
CD45.1 (donor)
WT
Empty
67.3%
30.4%
4.3%
94.4%
88.3%
11.2%
Tim4
CD45.1
CD206
D7 UV
TNFα
18.5%
79.7%
4.6%
93.3%
70.9%
26.7%
Tafa4 KO
9.6%
89.2%
19.1%
79.3%
82.1%
17.7%
g
Mo/Mϕ
tSNE1
tSNE2
CD45.1
Ly6C
MHC-II
CD64
CD206
TIM4
Expression Level
high
low
h
WT
Tafa4 KO
DN Mϕ
MHC-II+ Mϕ
Abs Nb DN Mac/mg skin
% CD45.1 DN Mac
Abs Nb MHC-II+ Mac/mg skin
% CD45.1 MHC-II+ Mac
No UV
D7 UV
i
DN Mϕ
MHCII+ Mϕ
Tim4+ Mϕ
D3 UV
DTR GINIP-DTR
cells
Annexin V
j
AnnexinV (Median MFI)
No UV
D3 UV
DTR
GINIP-DTR
k
D2 UV
WT Tafa4-KO
l
No UV
D2 UV
WT
Tafa4 KO

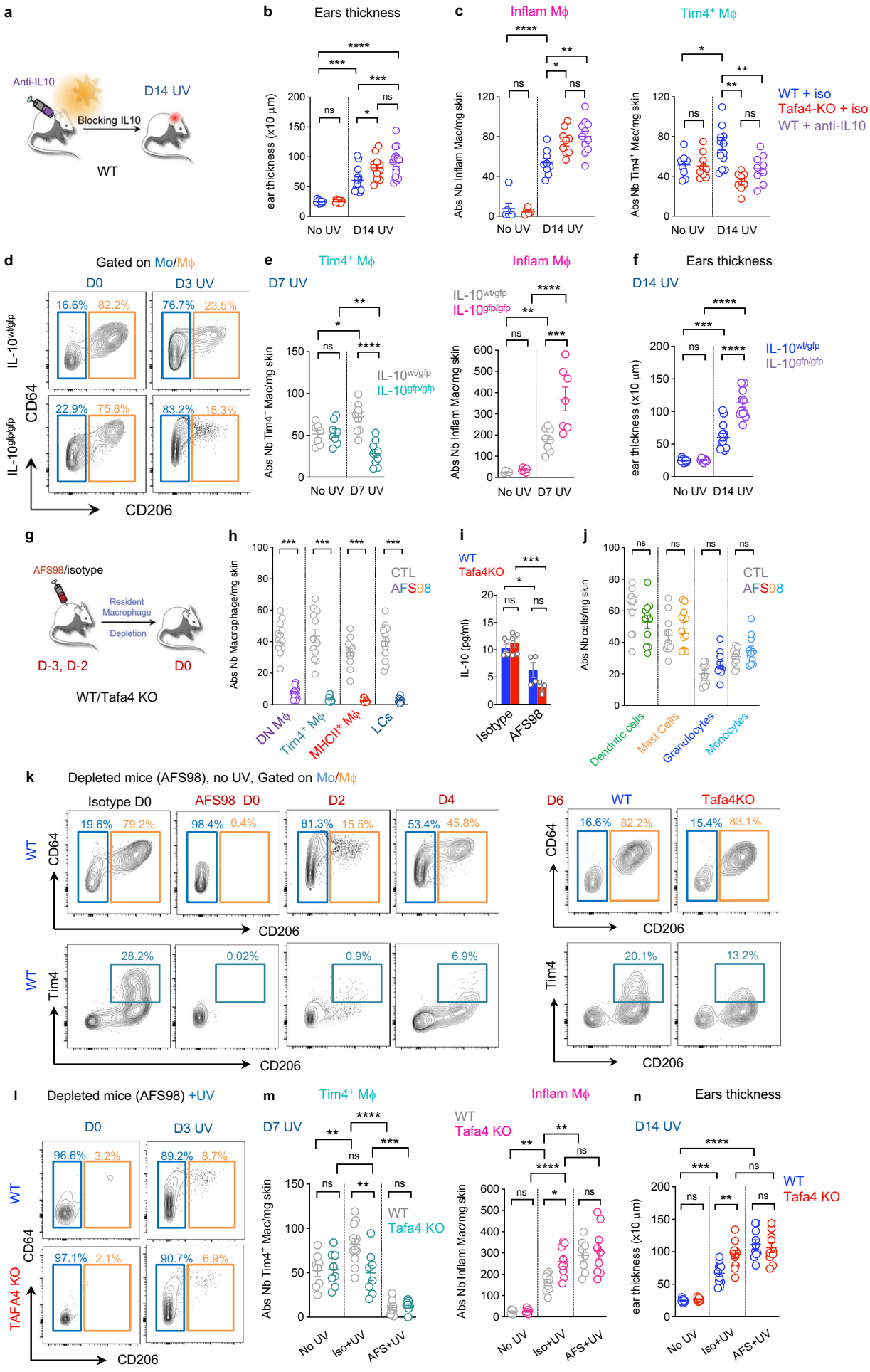
a
Anti-IL10
D14 UV
Blocking IL10
WT
b
Ears thickness
ear thickness (x10 µm)
No UV
D14 UV
c
Inflam Mϕ
Tim4⁺ Mϕ
Abs Nb Inflam Mac/mg skin
Abs Nb Tim4⁺ Mac/mg skin
WT + iso
Tafa4-KO + iso
WT + anti-IL10
d
Gated on Mo/Mϕ
D0
D3 UV
16.6%
82.2%
76.7%
23.5%
22.9%
75.8%
83.2%
15.3%
IL-10wt/gfp
IL-10gfp/gfp
CD64
CD206
e
Tim4⁺ Mϕ
D7 UV
Inflam Mϕ
Abs Nb Tim4⁺ Mac/mg skin
Abs Nb Inflam Mac/mg skin
No UV
D7 UV
f
Ears thickness
D14 UV
ear thickness (x10 µm)
g
AFS98/isotype
Resident Macrophage Depletion
D-3, D-2
D0
WT/Tafa4 KO
h
Abs Nb Macrophage/mg skin
CTL
AFS98
DN Mϕ
Tim4⁺ Mϕ
MHCII⁺ Mϕ
LCs
i
WT
Tafa4KO
IL-10 (pg/ml)
Isotype
AFS98
j
Abs Nb cells/mg skin
Dendritic cells
Mast Cells
Granulocytes
Monocytes
k
Depleted mice (AFS98), no UV, Gated on Mo/Mϕ
Isotype D0
AFS98 D0
D2
D4
D6
WT
Tafa4KO
19.6%
79.2%
98.4%
0.4%
81.3%
15.5%
53.4%
45.8%
16.6%
82.2%
15.4%
83.1%
Tim4
28.2%
0.02%
0.9%
6.9%
20.1%
13.2%
l
Depleted mice (AFS98) +UV
TAFA4 KO
96.6%
3.2%
89.2%
8.7%
97.1%
2.1%
90.7%
6.9%
m
Tim4⁺ Mϕ
D7 UV
Inflam Mϕ
WT
Tafa4 KO
No UV
Iso+UV
AFS+UV
n
Ears thickness
D14 UV

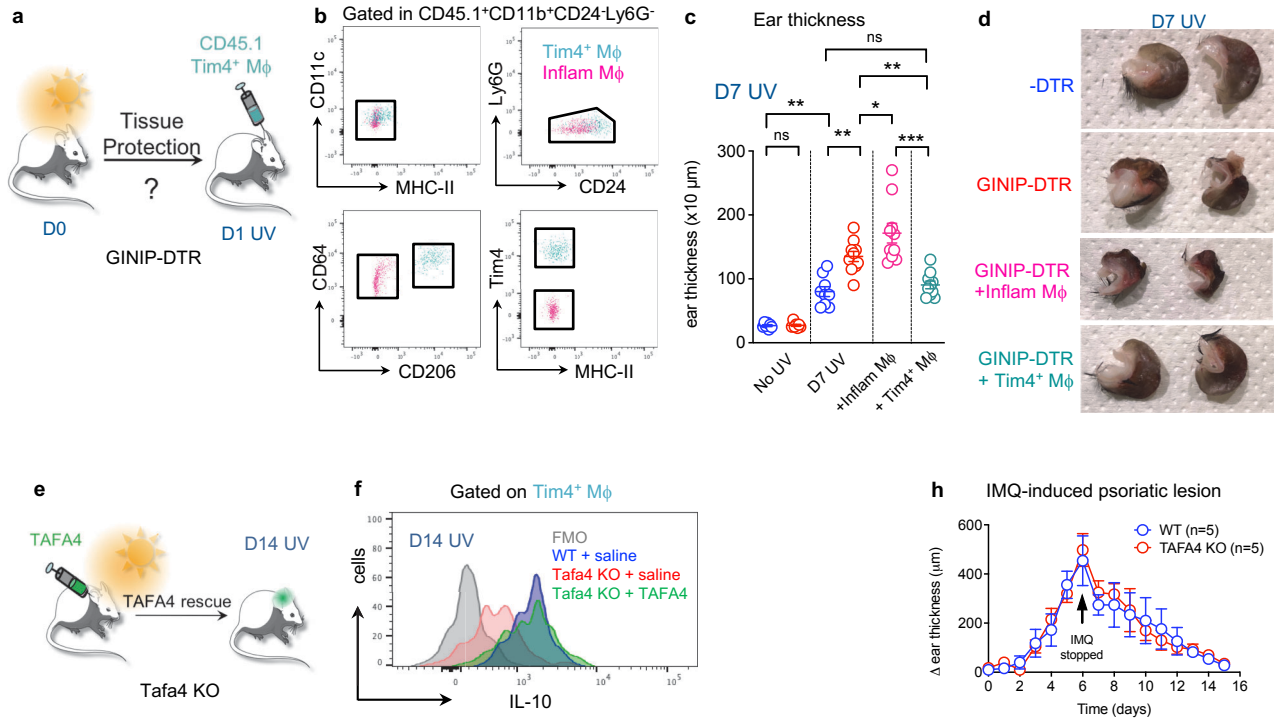

g Model

1) Role of TAFA4 during the Inflammatory phase

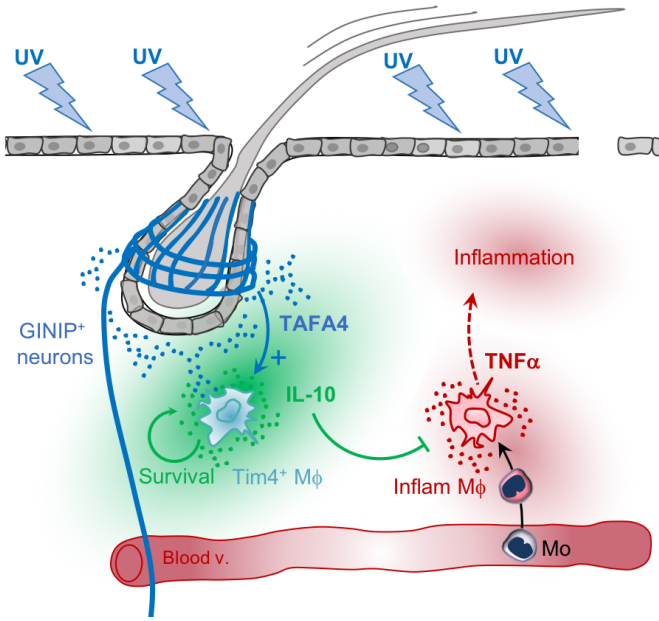

2) Role of TAFA4 during the Resolution phase